Template-assembled melittin: Structural and functional characterization of a designed, synthetic channel-forming protein

MICHAEL PAWLAK,[1] ULRICH MESETH,[1] BOOPATHY DHANAPAL,[2]
MANFRED MUTTER,[2] AND HORST VOGEL[1]

[1] Institute of Physical Chemistry IV, Swiss Federal Institute of Technology Lausanne, Lausanne, Switzerland
[2] Institute of Organic Chemistry, University of Lausanne, Lausanne, Switzerland

Abstract

Template-assembled proteins (TASPs) comprising 4 peptide blocks, each of either the natural melittin sequence (melittin-TASP) or of a truncated melittin sequence (amino acids 6–26, melittin$_{6-26}$-TASP), C-terminally linked to a (linear or cyclic) 10-amino acid template were synthesized and characterized, structurally by CD, by fluorescence spectroscopy, and by monolayer experiments, and functionally, by electrical conductance measurements on planar bilayers and release experiments on dye-loaded vesicles. Melittin-TASP and the truncated analogue preferentially adopt α-helical structures in methanol (56% and 52%, respectively) as in lipid membranes. Unlike in methanol, the melittin-TASP self-aggregates in water. On an air–water interface, the differently sized molecules can be self-assembled and compressed to a compact structure with a molecular area of around 600 Å^2, compatible with a 4-helix bundle preferentially oriented perpendicular to the interface. The proteins reveal a strong affinity for lipid membranes. A partition coefficient of 1.5×10^9 M^{-1} was evaluated from changes of the Trp fluorescence spectra of the TASP in water and in the lipid bilayer. In planar lipid bilayers, TASP molecules are able to form defined ion channels, exhibiting a small single-channel conductance of 7 pS (in 1 M NaCl). With increasing protein concentration in the lipid bilayer, additional, larger conductance states of up to 1 nS were observed. These states are likely to be formed by aggregated TASP structures as inferred from a strongly voltage-dependent channel activity on membranes of large area. In this respect, melittin-TASP reveals channel features of the native peptide, but with a considerably lower variation in the size of the channel states. Compared to the free peptide, template-assembled melittin has a much higher membrane activity: it is about 100 times more effective in channel formation and 20 times more effective in releasing dye molecules from lipid vesicles. This demonstrates that the lytic properties are not solely related to channel formation.

Keywords: dye release; monolayer assembly; planar lipid bilayers; protein aggregation; protein folding; protein-lipid affinity; reconstitution; voltage-dependent ion channels

Channel-forming membrane proteins play a central role in biological signal-transduction processes (Hille, 1992). In spite of tremendous efforts, only a single class of channel proteins has been structurally elucidated at the atomic level — the porins of the outer membrane of bacteria. These proteins are folded to form a closed β-barrel in which the amphipathic β-strands create a hydrophilic pore, leaving the protein's outer surface hydrophobic for inserting and traversing the apolar part of a lipid bilayer (Weiss et al., 1991; Cowan et al., 1992). In the case of ligand- and voltage-gated ion channels, no high-resolution protein structure is available yet. There is an ongoing debate as to whether the channel-forming part in these proteins might be formed by amphipathic or hydrophobic, bilayer-spanning α-helices and/or β-strands (Akabas et al., 1992; Changeux et al., 1992; Durell & Guy, 1992; Miller, 1993; Unwin, 1993a, 1993b; Görne-Tschelnokow et al., 1994).

An important concept for investigating the structure–function relationship of protein channels is the design of artificial channels either by genetic engineering of mutant proteins (Imoto et al., 1988; Numa, 1989) or by chemical synthesis of short peptides of about 20–30 amino acids of simplified sequences (Menestrina et al., 1986; Lear et al., 1988; Vogel et al., 1993) and of sequence stretches of authentic proteins (Montal, 1990 and references therein). The studies with mutant proteins have yielded substantial information on which part of the protein sequence might be involved in channel formation. In addition, the work with synthetic peptides showed that certain sequence motifs might be responsible for the channel formation. In particular, peptides that may traverse the lipid bilayer as amphipathic α-helix bundles are candidates to be involved in a channel structure (Montal, 1990; Åkerfeldt et al., 1993). Other channel-structure motifs are flexible elements such as bends in membrane-traversing α-helices (Vogel et al., 1993). Certain naturally occurring peptides, like alamethicin, melittin, or magainins, show similarities in their structural and channel-forming properties (Boheim & Kolb, 1978; Tosteson & Tosteson, 1981; Hanke et al., 1983; Vogel, 1987; Duclohier et al., 1989). Functional ion channels of these short and amphiphilic peptides are thought to be formed not by single molecules, but by membrane-spanning homo-oligomers including a spectrum of different stoichiometries. The channels can be activated upon application of a transmembrane electric field, thus involving structural transitions of the individual peptide molecules within the lipid membrane. Changes of peptide orientation, conformation, and aggregation have to be considered (Sansom, 1991; Chung et al., 1992; Hille, 1992), but even in such apparently simple cases, it has not been possible till now to determine experimentally the channel structure or the gating process. In principle, the structural transitions of the polypeptides in the process of channel activation might also occur in natural proteins, but it has not yet been established to what extent these processes are biologically relevant.

To more closely model natural channel proteins, template-assembled synthetic proteins have been created, comprising bundles of individual channel-forming polypeptides attached to a hydrophilic template. This mode of attachment reduces the translational, rotational, and internal degrees of freedom of the individual peptides, which therefore might adopt a different conformation compared to the free, monomeric, or autoaggregated state. The main goal of the TASP-approach is that the template serves to induce and direct the intramolecular folding of the amphiphilic peptide blocks into an α-helix-bundle topology. This topology might enable a single TASP-molecule to form an ion-channel structure. In several examples, it has been shown that TASPs with selected amino acid sequences of natural protein channels, as well as with designed sequences, can reconstitute channel activity in planar lipid bilayers. This fact could be explained in the framework of the above-mentioned concept (Montal et al., 1990; Åkerfeldt et al., 1992; Grove et al., 1993a, 1993b). However, a detailed structural investigation of channel-forming TASPs and, more importantly, the way in which a certain structure is correlated to a particular channel state have not yet been performed.

Here we present a detailed investigation of this kind. As model compounds, we have constructed 4α-helix-bundle TASPs comprising either the sequence of native melittin (melittin-TASP) or shorter melittin fragments (amino acids 6–26, melittin$_{6-26}$-TASP) (Fig. 1). Melittin itself, a 26-amino acid peptide from bee

$$(+) \qquad + \qquad ++++$$
$$\boxed{\text{N} \quad \text{melittin}} = \text{GIGAVLKVLTTGLPALISWIKRKRQQ}$$
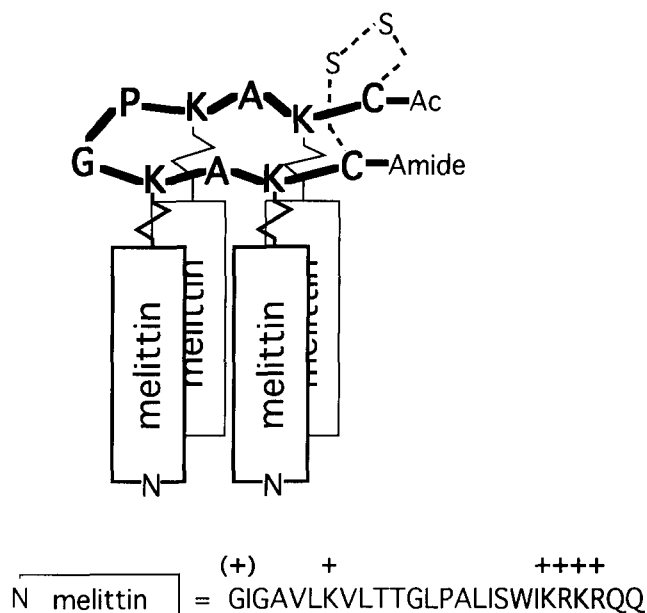
Fig. 1. A sequence representation of melittin-TASP. Four blocks of melittin are C-terminally linked to the ϵ-NH$_2$ groups of the lysine (K) side chains of a 10-amino acid template. The template could be cyclized via S–S bond formation of the 2 cysteines (C). The amino acid sequence of melittin is shown in 1-letter code starting with the N-terminal glycine (G). The electrical charges of the amino acid side chains and the N-terminus at neutral pH are indicated. The N-terminus of melittin corresponds to N.

venom, induces channel activity in lipid bilayers that is thought to be dominated by the formation of tetrameric α-helix bundles (Tosteson & Tosteson, 1981; Pawlak et al., 1991). Both the electrical properties of the polypeptide channels and the structural characteristics of melittin have been the subject of intensive research during the last 15 years (for a review, see Dempsey, 1990). Most importantly, the 3-dimensional structure of melittin is known to high resolution, derived from crystals grown in aqueous environment. According to the X-ray diffraction analysis (Terwilliger & Eisenberg, 1982; Terwilliger et al., 1982), the peptide forms a bent α-helix with a proline-induced kink between amino acids 10–11 (see Fig. 1 for the peptide sequence). The helix from amino acids 1 to 20 is amphipathic, with a polar convex surface and an apolar concave surface. This structural motif of the peptide is mainly preserved in the tetrameric state in aqueous solutions, in monomers in organic solutions, and bound to lipid micelles or bilayers (Vogel & Jähnig, 1986; Vogel, 1987; Bazzo et al., 1988; Inagaki et al., 1989). In this respect, melittin-TASP is an attractive example to test the TASP concept in general, and the structure–function relationship of one of the best characterized channel-forming peptides in particular.

Melittin-TASP and its shorter peptide fragment analogue melittin$_{6-26}$-TASP were prepared by stepwise solid-phase peptide synthesis, starting with a 10-amino acid template Ac-C$\underline{\text{K}}$ A$\underline{\text{K}}$PG$\underline{\text{K}}$A$\underline{\text{K}}$C-NH$_2$ to which the 4 peptide blocks were coupled via their C-terminal ends to the ϵ-amino groups of the underlined lysines (Dhanapal et al., 1993). Both a linear and a cyclized (disulfide-bridged at both Cys) template were used to construct melittin-TASPs. The template was designed to adopt 2 anti-

parallel KAK β-strands connected by a β-turn to locate the amphiphilic peptide blocks on 1 side. This concept offers the possibility of folding into a 4α-helix bundle topology as shown schematically in Figure 1 (Mutter & Vuilleumier, 1989; Mutter et al., 1992). The structures of melittin-TASP in different solvents as well as in lipid bilayers were investigated by optical spectroscopy. CD was applied to measure the ensemble-averaged polypeptide conformation. For the reconstitution of functional ion channels in lipid bilayers, a reasonably strong interaction of the particular proteins with the membrane is required. Therefore, the affinity of melittin-TASP to lipid membranes was derived quantitatively by evaluating the changes of the Trp fluorescence at different concentrations of lipid. Pressure-area isotherms of melittin-TASP monolayers on the water surface of a Langmuir trough were studied in order to obtain information on the orientation of protein molecules under conditions comparable to a membrane–water interface. The channel formation characteristics and the overall membrane activity of melittin-TASP were investigated in planar lipid bilayers and dye-loaded lipid vesicles. Different reconstitution protocols were tested for their influence on the final channel activity and to relate the functional changes to the structural preconditions in the different solvent systems. In addition, a number of modified TASP molecules were synthesized in order to investigate whether structural and/or channel-forming properties were changed compared to melittin-TASP: (1) melittin-TASP comprising a cyclized template, (2) acetylated melittin-TASP, where the positive charges of the melittin segments are blocked by acetylation, and (3) a truncated form melittin$_{6-26}$-TASP. A preliminary part of this work has already been presented (Dhanapal et al., 1993; Meseth et al., 1993).

Results[3]

CD studies

The solubility of melittin-TASP was high in methanol, but considerably lower in more polar (water) or less polar (ethanol) environments. It was nearly insoluble in isopropanol. We first measured the CD of the melittin-TASP in methanol. The spectrum is typical of a preferential α-helical conformation, as shown in Figure 2. The mean residue ellipticity at 222 nm, $[\theta]_{222}$, characteristic of the α-helix content, was $-15,200$ deg cm^2 dmol^{-1} (Table 1). From this we can estimate an α-helix content of 56% for the TASP-molecule in methanol, which corresponds to 14–15 amino acid residues per melittin segment in an α-helix conformation.[4] The linear and cyclic variants of the protein showed

---

[3] If not otherwise indicated, the results correspond to the noncyclized melittin-TASP and melittin$_{6-26}$-TASP (no Cys–Cys disulfide bonds). Experiments performed with the cyclized TASP are indicated explicitly.

[4] We are aware of the fact that the absolute percentage of helix content depends on several parameters that are more or less defined, such as protein concentration (uncertainty $\pm 5\%$), chosen reference state of 100% helix, or chosen method of evaluation of the secondary structure from CD spectra (see Vogel, 1987), as well as conformational fluctuations of the polypeptides (Vogel et al., 1988). The helical parts of the TASP were assumed to be located exclusively in the melittin peptide blocks because the template should adopt only a β-strand/β-turn structure (Mutter et al., 1992). In the present context, the average percentage of helix content is used as a measure to compare the structures of different peptides within the same framework of CD results (see Table 1).
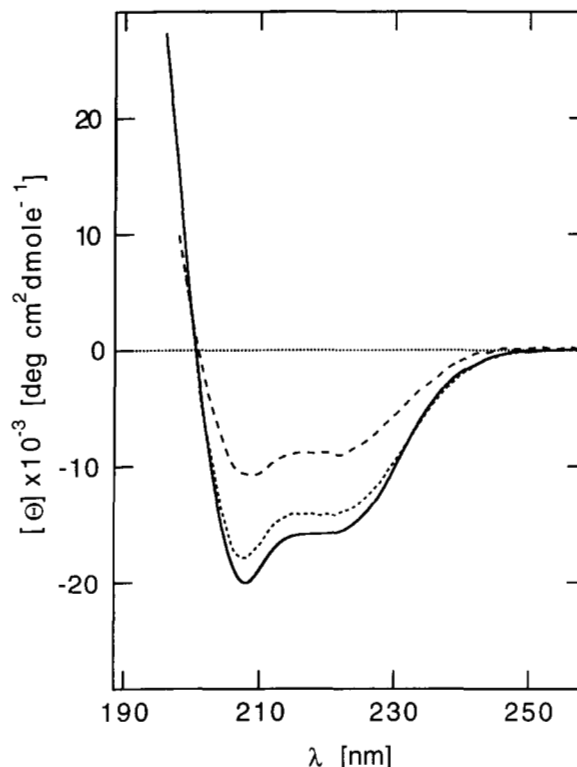
Fig. 2. CD spectra showing the mean residue ellipticities of melittin-TASP in methanol (——) and in 10 mM Tris-HCl, pH 7.4 (– – –). The protein concentrations were 21 μM in methanol (optical pathlength = 1 mm) and 0.7 μM in aqueous buffer (optical pathlength = 10 mm). In aqueous buffer, spectra were recorded 1 min after protein addition from a concentrated protein solution in methanol. For a comparison, the spectrum of the shorter analog melittin$_{6-26}$-TASP (·····) in methanol is shown (protein concentration = 60 μM, optical pathlength = 1 mm). The temperature was always maintained at 25 °C.

comparable signals. The conformation of the TASP was stable, i.e., CD spectra could be reproducibly recorded over a time range of 2 h.

CD spectra in aqueous solution were obtained after adding small aliquots of a concentrated protein solution in methanol to a cuvette containing 10 mM Tris-HCl, pH 7.4. The samples were always well stirred. A typical α-helix spectrum was still obtained (Fig. 2), but with a concentration-dependent lower mean ellipticity per residue (Table 1). At 0.7 μM melittin-TASP, an α-helix content of 33% was observed. The spectra, however, were not stable: after the protein was added to the buffer, the ellipticity decreased continuously by between 10% and 20% of the initial signal, reaching an apparent stationary value after 1 h. Simultaneous measurements of the UV-absorption spectra revealed an increase of scattered light with comparable kinetics. Furthermore, the time-dependent spectral changes were more pronounced in the presence of 100 mM NaCl, where the solution became highly turbid after some time. Such a behavior indicates strong protein aggregation in solution.

Protein aggregation, like protein structure, critically depends on the environmental solvent. For this reason, CD spectra of the melittin-TASP were measured over a wide range of concentrations, in methanol and in aqueous 10 mM Tris-HCl, pH 7.4. Figure 3 shows the concentration dependence of $[\theta]_{222}$ values.

Table 1. *Mean residue ellipticities of melittin-TASP, melittin$_{6-26}$-TASP, and melittin at 222 nm, $[\theta]_{222}$, under different experimental conditions*[a]

	$[\theta]_{222}$ (deg·cm²·dmol⁻¹)[b]	Signal stability	% Helix content (n_α)[c]
Melittin-TASP			
In methanol	−15,200	Stable	56 (14–15)
In methanol/POPC	−15,300	Stable	56 (14–15)
In water	−9,100	Decreasing	33 (8–9)
In water/POPC (SUV or LUV)[d]	−7,200[e]	Decreasing	
In water/POPC (methanol injection)[f]	−15,600	Slightly decreasing	57 (15)
Melittin$_{6-26}$-TASP			
In methanol	−14,000	Stable	52 (10–11)
Melittin			
In water/DTPC (Vogel, 1987)	−23,200	Stable	77 (20)

[a] Protein concentration was 0.7 µM for melittin-TASP (optical pathlength = 10 mm) and 60 µM for melittin$_{6-26}$-TASP (optical pathlength = 1 mm). Ellipticities were measured 1 min after the addition of protein and/or lipid. Signals are baseline-corrected for the contribution of the lipid vesicles. Water corresponds to 10 mM Tris-HCl, pH 7.4. Temperature was kept at 25 °C.

[b] ±5%.

[c] Percentage of α-helix content and n_α, average number of amino acid residues per peptide block in an α-helical conformation; the helical part was assumed to be located exclusively in the melittin peptide blocks because the template should only adopt a β-turn structure (see footnote 4).

[d] SUV or LUV of POPC were added to a freshly prepared protein solution in aqueous buffer (L:P = 800).

[e] Lipid was added 10 min after protein addition; the subsequent measurement did not show a change in ellipticity.

[f] Small amounts of a concentrated solution of lipid and protein (L:P = 800) in methanol were injected into aqueous buffer.

Because the signals changed with time, spectra in aqueous buffer were always taken 1 min after protein addition. $[\theta]_{222}$ remained constant in methanol, which is indicative of a stable conformation in that solvent. In water, however, the ellipticity was strongly dependent on the final protein concentration: the absolute signal increased with the amount of protein added. We therefore conclude that the TASP adopts a stable monomeric state in methanol but has a strong tendency to aggregate in an aqueous environment. Aggregation is greatly promoted by increasing protein concentration and salt content.

CD spectra of melittin-TASP were also measured in the presence of lipid. The addition of 1 mg/mL POPC to methanol did not change the ellipticity of the protein when compared with pure methanol (Table 1). Addition of POPC vesicles (SUV or LUV) to a freshly prepared protein solution (0.7 µM) in 10 mM Tris-HCl, pH 7.4, up to final lipid:protein ratios of L:P = 1,000 had virtually no influence on the CD signal (Table 1). Either no protein associated with the lipid vesicles under these conditions, or no conformational change of the protein upon lipid association could be observed. We therefore applied a different method for membrane insertion of the TASP: small aliquots of a solution of a defined L:P composition in methanol were diluted by injection into the aqueous buffer, reaching the same
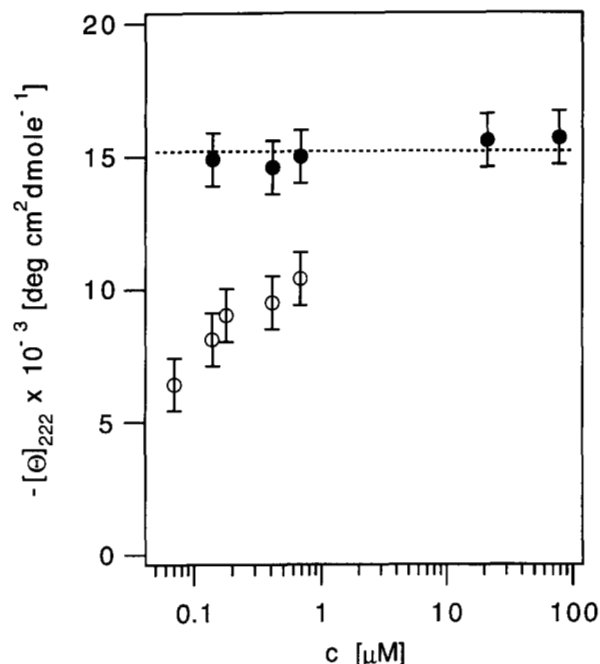
Fig. 3. Concentration dependence of the mean residue ellipticities at 222 nm, $[\theta]_{222}$, for melittin-TASP in methanol (●) and in 10 mM Tris-HCl, pH 7.4 (○). Error bars correspond to standard deviations from different experiments ($n = 3$). Signals were stable in methanol (the dotted line corresponds to the averaged value −15,200 deg cm² dmol⁻¹). In aqueous buffer, the absolute signal decreased by 10–20% over 1 h. The values in 10 mM Tris-HCl are therefore recorded 1 min after protein addition. The temperature was kept at 25 °C.

final protein concentration as before. The observed values of $[\theta]_{222}$ of this preparation were comparable to the values of melittin-TASP in pure methanol. Clearly, the protein was able to associate with the lipid membrane stabilizing its secondary structure because the kinetics of the CD spectral changes were much slower. Due to the small change in secondary structure upon lipid association, however, the CD signal is not suitable for quantification of the affinity of template-assembled melittin to lipid membranes. In this respect, melittin-TASP behaves differently from native melittin. For the latter, a dramatic conformational change was observed from a nonregular state in aqueous solution (at low peptide concentration and ionic strength) to a preferential α-helical structure in lipid membranes (Vogel, 1981).

Finally, melittin$_{6-26}$-TASP was characterized by CD. The 52% helix content determined corresponds to an average of about 11 amino acid residues per peptide block, distinctly lower than that found in melittin-TASP.[4]

Fluorescence measurements

Melittin-TASP in methanol, excited at 280 nm, showed a Trp emission spectrum with a maximum at 348 nm. After a small, initial decrease of intensity shortly after protein dilution into a freshly cleaned quartz cuvette, the fluorescence signal remained stable. The initial signal decrease could be repeatedly observed after transferring the previously measured sample to a freshly cleaned cuvette. From this observation, we conclude that

melittin-TASP has a tendency to adsorb on quartz surfaces. After adding the protein to aqueous 10 mM Tris-HCl, pH 7.4, the fluorescence revealed a strongly time-dependent behavior: it lost about 30% of its intensity within the first minutes (Fig. 4, trace a). The kinetics of the fluorescence signal hardly changed upon titration of lipid vesicles (SUV of POPC) to the cuvette. In accordance with the CD measurements, the fluorescence signal was stable on injection of small amounts of a lipid:protein solution in methanol into the aqueous buffer (Fig. 4, trace b). The signal intensity increased but was rather insensitive to the lipid-to-protein ratio. However, the wavelength of maximum fluorescence, λ_{max}, was stable in time, with and without lipid, and revealed a continuous blue shift with increasing lipid:protein ratio from $\lambda(0) = 356.2 \pm 0.5$ nm (L:P = 0, equal to pure protein in solution) to $\lambda(\infty) = 350.2 \pm 0.5$ nm (estimated from a value taken at L:P = 1,000). Figure 5A shows the variation of λ_{max} with increasing lipid:protein ratio. The values of λ_{max} were determined from Gaussian fits to corresponding fluorescence spectra around their maxima.

Schwarz & Beschiaschvili, 1988). Here, the blue shift of λ_{max} (Fig. 5A) was used to evaluate the lipid affinity of melittin-TASP. We assume that, at the moment of sample injection, only 1 state of the protein (monomeric or aggregated) equilibrates between the aqueous and the lipid bilayer. Protein molecules in water may further self-aggregate or adsorb to the glass walls, resulting in changes of fluorescence intensity, as observed. However, these postinjection processes apparently do not influence λ_{max}. Therefore, all TASP molecules that are not lipid associated will be included in a term called "free" protein concentration, c_f.

The association of polypeptides to lipid membranes has been quantitatively evaluated in the literature in terms of a partition equilibrium between the aqueous and the lipid bilayer phase for melittin (Schwarz et al., 1986; Schwarz & Beschiaschvili, 1989; Beschiaschvili & Seelig, 1990) and for other pore-forming peptides (Rapoport & Shai, 1991; Peled & Shai, 1993; Schwarz & Blochmann, 1993). Here we apply this concept to melittin-TASP
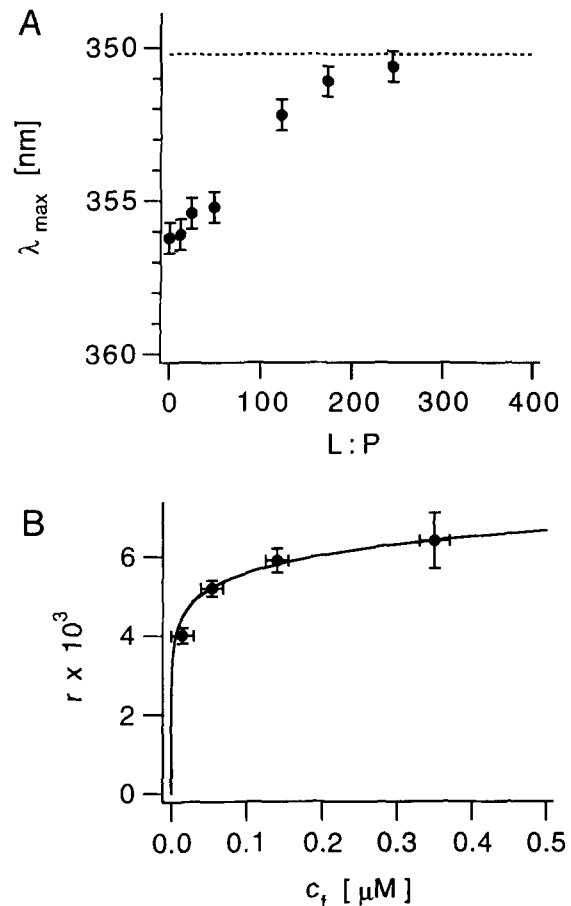
Lipid affinity

Wavelength shifts of the maximum fluorescence have already been shown in the literature to describe the monomer–tetramer association and the lipid partitioning of native melittin (Dufourcq & Faucon, 1977; Vogel, 1981; Quay & Condie, 1983;
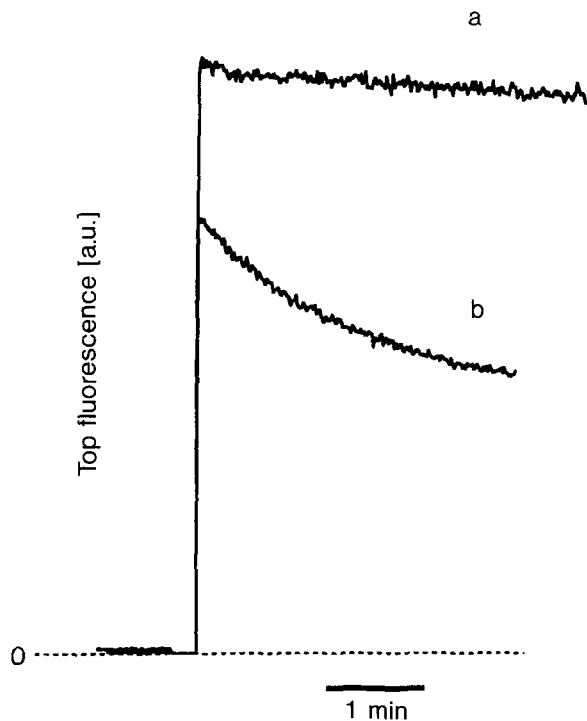
Fig. 4. Trp fluorescence of melittin-TASP upon injecting small and identical amounts (a) of a concentrated protein/methanol solution and (b) of a concentrated protein:lipid (POPC) solution in methanol into aqueous 10 mM Tris-HCl, pH 7.4 (excitation 280 nm, emission 350 nm). The final protein concentration was 0.5 μM, L:P = 240. The signal increased and was greatly stabilized in the presence of lipid.

Fig. 5. A: Shift of the wavelength at maximum fluorescence, λ_{max}, of melittin-TASP at increasing ratios of L:P (protein concentration = 0.5 μM), diluted from a concentrated methanol solution into 10 mM Tris-HCl, pH 7.4. The lipid was POPC. The dotted line indicates $\lambda(\infty) = 350.2$ nm, estimated from λ_{max} measured at L:P = 1,000. **B:** Association isotherm showing $r = c_{as}/c_l$ versus the "free" protein concentration c_f (the last 2 points at high c_f were omitted because of the large errors in calculating r). The solid curve is a fit using the lipid affinity $\Gamma = 1.5 \times 10^9$ M^{-1} and an effective charge number $z_{eff} = 5.2$ (cf. Equations 1, 4).

using the formalism of Schwarz et al. (1986). A partition coefficient Γ is defined according to[5]

$$r \cdot f(r) = \Gamma \cdot c_f, \tag{1}$$

with $r = c_{as}/c_l$ being the molar ratio of lipid-associated protein molecules per lipid molecule. $f(r)$, the activity coefficient as a function of r, may describe deviations from ideal partitioning ($f = 1$) due to protein–protein interaction at the water–membrane interface. The mole fractions of lipid-associated per total melittin-TASP, c_{as}/c_p, were taken from the individual shifts of maximum wavelength, λ_{max}, of Figure 5A by applying

$$c_{as}/c_p = r \cdot c_l/c_p = [\lambda(0) - \lambda_{max}]/[\lambda(0) - \lambda(\infty)], \tag{2}$$

and by using mass conservation,

$$c_p = c_{as} + c_f = r \cdot c_l + c_f, \tag{3}$$

the association isotherm of r versus the free protein concentration c_f (Equation 1) was constructed as shown in Figure 5B. A strong bending of the isotherm at increasing free protein concentrations is evident and indicates repulsive forces between the individual TASP molecules. As has been shown for net charged peptides such as melittin, the repulsive forces can be well described by electrostatic interaction if an effective electric charge $z_{eff} \cdot e$ (e = elementary electric charge) is attributed to each protein molecule (Schwarz & Beschiaschvili, 1989; Beschiaschvili & Baeuerle, 1991; Schwarz & Blochmann, 1993). The association of charged proteins to the membrane interface generates an electrical surface potential and further partitioning is restricted by the electrostatic repulsion between the free and already membrane-associated molecules. Applying the Gouy–Chapman approach (Hiemenz, 1986) to uniformly charged surfaces, the ac-

tivity coefficient $f(r)$ can be described as developed by Schwarz and Beschiaschvili (1989)

$$f(r) = \exp[2 \cdot z_{eff} \cdot \sin h^{-1}(z_{eff} \cdot b \cdot r)], \tag{4}$$

with z_{eff} being the effective charge number per protein molecule. b is an inherent parameter, which mainly depends on the salt content. A value of $b = 38.9$ corresponds to the present conditions of 10 mM ionic strength. Including the electrostatic expansion, the association isotherm of the TASP is now defined by 2 parameters: the partition coefficient, Γ, for the slope and the electric charge number, z_{eff}, for the bending of the isotherm.

A least-square fit of the isotherm (solid line of Fig. 5B) resulted in the following parameters:

$$\Gamma = 1.5 \pm 1.0 \times 10^9 \text{ M}^{-1} \ (6.0 \pm 1.0 \times 10^4 \text{ M}^{-1})$$

$$z_{eff} = 5.2 \pm 0.4 \ (1.9 \pm 0.1).$$

Published values for native melittin are shown in parentheses (Beschiaschvili & Seelig, 1990; Beschiaschvili & Baeuerle, 1991). Within our experimental errors, the value of Γ rather gives an estimation of the order of magnitude, whereas the curve bending was more critically dependent on z_{eff}. It should be noted that z_{eff} as an effective charge always remains below the physical valency z of the molecule (see Discussion). The values demonstrate 2 main characteristics of melittin-TASP when compared with free, monomeric melittin: firstly, a high, intrinsic affinity for lipid bilayers due to hydrophobic effects, and secondly, a strong intermolecular electrostatic repulsion perpendicular to the water–membrane interface that limits r to less than 1 bound molecule per 100 lipids. This is evident if one bears in mind that the TASP-protein has 4 positive charges at each of the C-terminal ends of the peptide blocks on the template side facing the aqueous environment. The 2 opposing effects may explain why the partitioning remains rather insensitive to L:P.

Monolayer experiments

Small amounts of a concentrated melittin-TASP solution in methanol were spread on the air–water interface (ca. 30 cm²) of a Langmuir trough.[6] The aqueous subphase was 10 mM Tris-HCl at pH 7.4. After waiting 1 h to allow the system to equilibrate, the TASP monolayer on the water surface was compressed and isotherms of surface pressure versus area per molecule were recorded. At a critical area of $A_c \approx 1,200$ Å² per molecule, a surface pressure was established and increased continuously up to almost 40 mN/m. The pressure remained stable at any fixed area, which indicates that the TASP molecules favor the air–water interface rather than diffusing into the bulk solution. Upon enlarging the surface area again, the monolayer pressure relaxed somewhat more slowly, leading to hysteresis of the isotherms. By allowing the system to relax for a sufficient time (about 1 h), the isotherms could be reproducibly observed. At a bilayer–monolayer equivalent pressure of 32 mN/m (Israelachvili et al., 1980), the area per molecule corresponded to 620 ± 60 Å². Pressure-area isotherms of the truncated analog

---

[5] The thermodynamic principle of a partition equilibrium of solute polypeptides between an aqueous and a lipid bilayer phase is equivalent to the concept developed by Tanford to describe the partitioning of small molecules (alkanes, amino acids, amphiphiles) between water and nonpolar solvents such as hydrocarbons, aliphatic alcohols, or lipid bilayers in particular (Tanford, 1980). These basic thermodynamic principles were shown later to be applicable to the quantification of polypeptide insertion into lipid bilayers, for example, the insertion of amphipathic apolipoproteins (reviewed by Massey & Pownall, 1986) or pore-forming peptides. In the latter cases, the physicochemical states of the polypeptides in water (w) or lipid (l) were defined by their thermodynamic chemical potentials

$$\mu_w = \mu_w^O + RT \cdot \ln(c/c_O)$$

$$\mu_l = \mu_l^{\bullet} + RT \cdot \ln(f \cdot r)$$

where c/c_O denotes the concentration of the polypeptides in water as the molar ratio per unit concentration ($c_O = 1$ M), r the molar ratio of lipid-associated molecules per lipid, and f an activity coefficient describing the peptide–peptide interactions at the interface. μ_w^O and $\mu_l^{\bullet}$ are the standard molar free energies of the molecule at infinite dilution. At equilibrium ($\mu_w = \mu_l$), the ratio of solute molecules associated with the lipid and in the water phase is determined by the partition coefficient Γ, defined as $\Gamma = 1/c_O \cdot \exp(-\Delta G_{as}^O/RT)$ (unit: M^{-1}) with $\Delta G_{as}^O = \mu_l^{\bullet} - \mu_w^O$, the difference between the standard chemical free energies of the 2 phases.

[6] The design of the Langmuir trough is described by Lang et al. (1994). Experimental details will be published elsewhere.

melittin$_{6-26}$-TASP showed comparable behavior, and the area per molecule at 32 mN/m was only slightly reduced (590 ± 60 Å^2).

Planar bilayer experiments

Macroscopic current-voltage curves

Small amounts of a melittin-TASP solution in methanol were added in close proximity to 1 side of preformed, large BLMs of DOPC. The final protein concentrations in solution were in the nanomolar range. Stationary current–voltage curves (I-V curves) were recorded 1 h after protein addition (Fig. 6). As for native melittin, the voltage and concentration dependence of the protein-induced membrane conductance, G, can be described according to Latorre and Alvarez (1981)

$$G = g_O \cdot c_p^m \cdot \exp(\alpha \cdot eV/kT). \qquad (5)$$
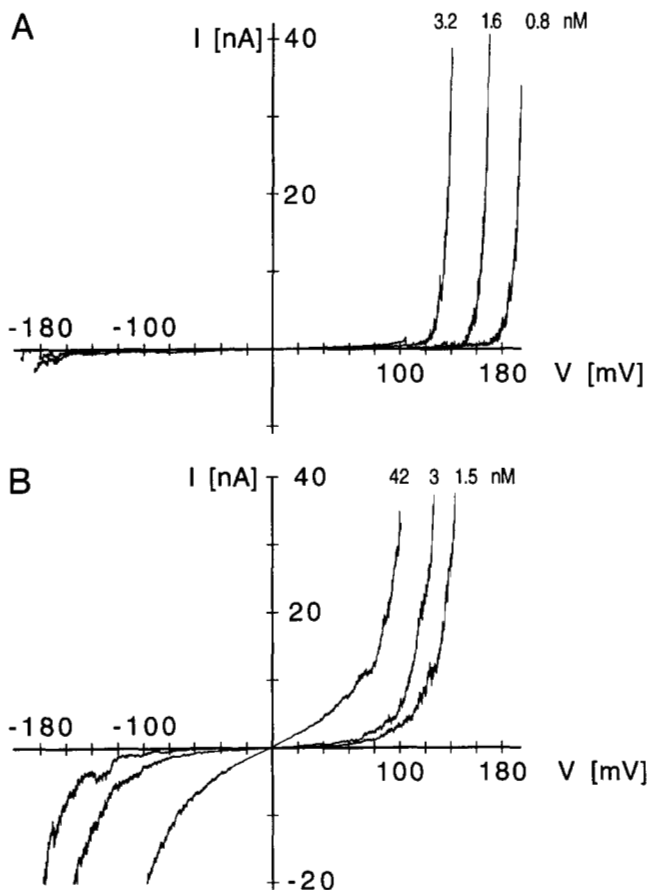
Fig. 6. Stationary current–voltage curves induced by melittin-TASP in 1 M NaCl, 10 mM Tris-HCl, pH 7.4, on large, decane-containing BLMs of DOPC, recorded upon application of linear voltage ramps (100 mV/min). The curves were recorded ~1 h after adding the protein from a (**A**) high (15 μM) or (**B**) low (1.5 μM) concentrated stock solution in methanol to the electrolyte of 1 side of the bilayer membrane (*cis*). Positive voltage corresponds to the *cis* side (*trans* being grounded). The characteristic number of gating charges α (corresponding to the voltage per e-fold conductance increase, Equation 5) were $\alpha = 5.2$ for A and 1.4 for B. Curves at increasing final protein concentrations (indicated) followed a power law (Equation 5) dependence with mean aggregation numbers $m = 6$-8 (A) and $m \simeq 1$ (B).

This expression includes a power law dependence of the protein concentration c_p, with m being the mean aggregation number, i.e., the mean number of molecules within a channel aggregate. The exponential voltage dependence includes the characteristic number of gating charges α (or equivalent dipole contributions) being moved across the membrane during channel activation. kT/e denotes the thermal energy per electric elementary charge e ($kT^{298K}/e = 26$ mV). g_O is an inherent parameter dependent on the ionic strength, pH, etc. The evaluated parameters m and α of melittin-TASP are listed in Table 2 and compared to values of the native peptide under identical conditions (Pawlak et al., 1991).

Interestingly, the I-V curves showed different behavior when using a more (Fig. 6A) or less (Fig. 6B) concentrated protein stock solution. In the former case, the I-V curves were strongly concentration dependent ($m = 6$-8) and strongly voltage-dependent ($\alpha = 5.2$), but fully asymmetric concerning their voltage-induced activity: only positive voltages on the *cis* side could induce a current. In the latter case, the concentration dependence was almost linear ($m \simeq 1$), with a moderate voltage dependence ($\alpha = 1.4$). Membrane conductance could also be induced at negative voltages with only a slight asymmetry of activity. A comparable voltage dependence ($\alpha = 1.3$) and a small asymmetry in channel activity was also observed for the natural peptide (Pawlak et al., 1991). At higher concentrations of melittin-TASP only, a voltage-independent conductance appeared, clearly damaging the membrane by surface-active effects, but it was much less pronounced than for the free peptide. Most importantly, the total concentration of melittin-TASP in the aqueous phase (some nM), necessary to induce a particular channel conductance, was about 100 times less than for native melittin (Pawlak et al., 1991).

Single-channel measurements

Melittin-TASP. In order to reveal the single-channel characteristics of melittin-TASP, electrical current measurements with a high current resolution were performed on small, "virtually" solvent-free lipid bilayers of DOPE:DOPC (4:1) at the tips of glass pipettes (tip diameters were around 1 μm). Single transitions into distinct open states of different amplitudes, as well as multiple transitions resulting from mixtures of channel states, could be observed in different experiments or in one and the same experiment at different times of the current recordings. Figure 7 shows typical sections of current recordings of single and multiple transitions into the 3 predominant states (Fig. 7A,B,C). The channel characteristics were almost symmet-

Table 2. *Voltage and concentration dependence of stationary, macroscopic membrane conductance*[a]

	α	m
Melittin-TASP (Fig. 6A)	5.2 ± 0.5	6-8
Melittin-TASP (Fig. 6B)	1.4 ± 0.2	~1
Melittin (Pawlak et al., 1991)	1.3 ± 0.1	4

[a] The stationary, macroscopic membrane conductance was induced by melittin-TASP and melittin in large BLM of DOPC (1 M NaCl, 10 mM Tris-HCl, pH 7.4). Fitted from curves as shown in Figure 5 according to Equation 6.
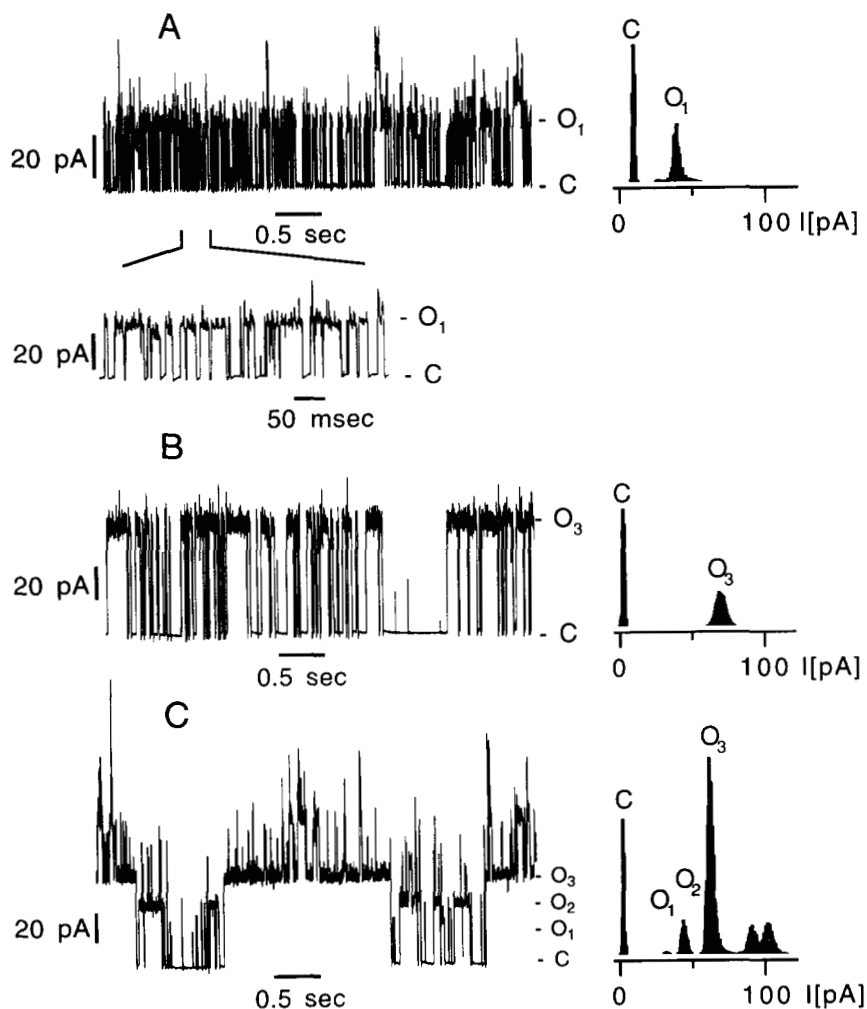
Fig. 7. Single-channel activity of melittin-TASP on small patch membranes of DOPE: DOPC (4:1) in symmetric 1 M NaCl, 10 mM Tris-HCl, pH 7.4, showing typical segments of current recordings of the 3 dominating channel states O_1 (600 pS), O_2 (935 pS), and O_3 (1,250 pS) and their frequency of occurrence-current histograms: (**A**) single transitions of O_1; (**B**) single transitions of O_3; and (**C**) multiple transitions of O_1, O_2, and O_3. Closed and open states are indicated by C and O, respectively. The membranes were assembled from monolayers that had been spread from a lipid: protein solution (L:P = 1,000) in chloroform. The applied voltage was 50 mV.

rical for different polarities of the applied voltages. In general, increasing the voltage activated more channels and also channels with larger current amplitudes. Thus, current traces at high voltages (>120 mV) became complex and difficult to evaluate.

The current amplitudes, $\langle I \rangle$, of the individual single-channel states of melittin-TASP were evaluated from Gaussian fits to current histograms at different voltages, comprising single and multiple transitions ($n = 18$). The results of the different experiments are summarized in Figure 8. Three different channel states (called O_1, O_2, O_3) can be clearly distinguished. They all reveal a small but significant voltage dependence of $\langle I \rangle$. To a first approximation, these voltage dependencies could be described exponentially with an e-fold increase every 110 ± 10 mV (Fig. 8, dotted lines). The single-channel conductances of these states were $\langle O_1 \rangle = 600 \pm 30$ pS, $\langle O_2 \rangle = 935 \pm 70$ pS, and $\langle O_3 \rangle = 1,250 \pm 130$ pS (all at 50 mV). $\langle O_3 \rangle$ is about twice $\langle O_1 \rangle$, but double openings into or double closings from O_3 could not be detected and the kinetics of O_1 and O_3 are markedly different (Fig. 7A,C; Table 3). In a few cases, channels of a smaller conductance (below 100 pS) have been observed with a low open probability.

Information on the gating kinetics of the melittin-TASP channels was derived by measuring the mean lifetimes (τ_{open}, τ_{closed})

for the open and closed states of the individual current states at different voltages. The data were obtained from monoexponential fits to lifetime histograms of current segments containing a large number of single transitions ($N \geq 200\text{-}1,000$, $n = 7$). The values of the exponential decay constants, τ_{open} and τ_{closed}, are summarized in Table 3 and were typically in the range of 10–100 ms. τ_{open} showed a tendency for longer times with increasing voltages, whereas τ_{closed} remained more or less constant.

Acetylated melittin-TASP. Single-channel measurements were performed with acetylated melittin-TASP ($n = 3$). At neutral pH, this TASP molecule has a drastically reduced net electric charge because positive charges of the free N-termini, Lys 7, Lys 21, and Lys 23 are removed. Thus, less repulsive forces are expected within a TASP bundle. With this TASP analogue, first-channel activity appeared only 15–30 min after membrane formation (Fig. 9, trace A). Current transitions occurred only to a long-lasting channel state, O* ($\tau_{open} \leq$ seconds), of 1 distinct amplitude. The channel conductance was small, $\langle O^* \rangle = 45 \pm 5$ pS, and ohmic (O* in Fig. 10). With time, channels of larger conductance appeared, similar to O_1, O_2, and O_3 of the unmodified melittin-TASP (600–1,000 pS). After 1 h, 2 main channel states were established, O_1^{ac} and O_2^{ac} (Fig. 9B,C), with con-
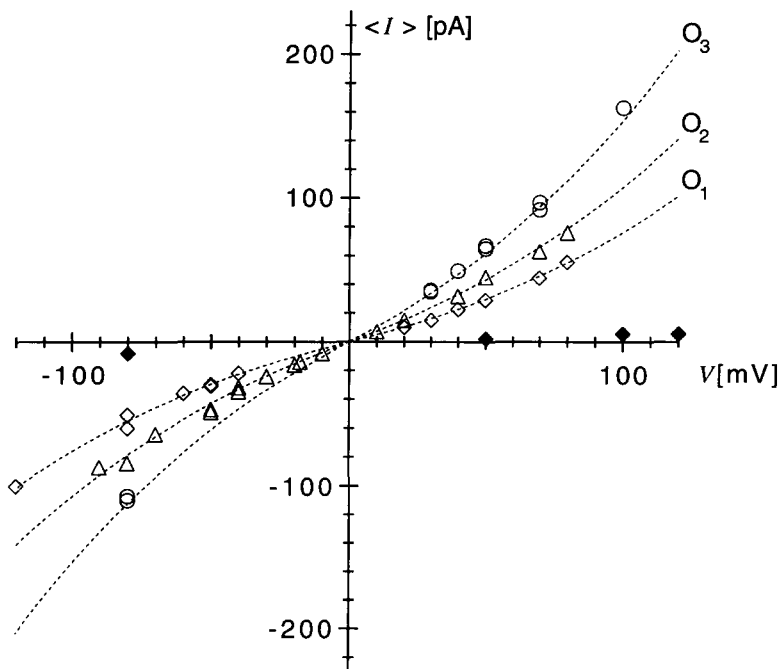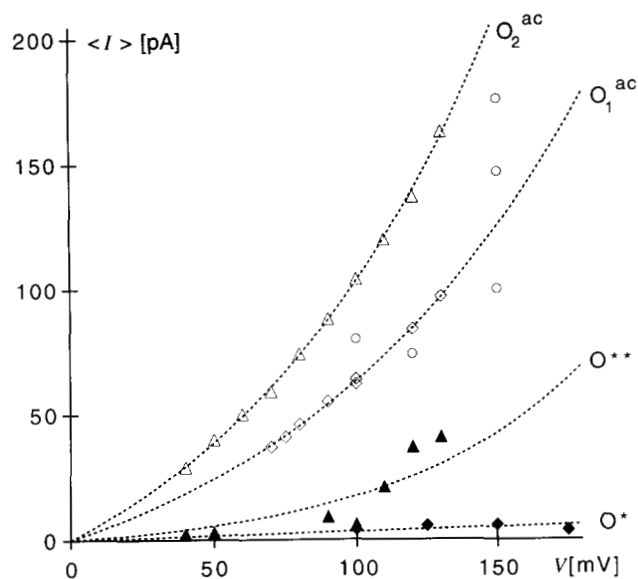
Fig. 8. Current–voltage characteristics of single-channel states formed by melittin-TASP on patch membranes of DOPE:DOPC (4:1) in 1 M NaCl, 10 mM Tris-HCl, pH 7.4. Open markers represent mean single-channel currents evaluated from Gaussian fits to current histograms of channel trace sections, which contained at least 400 events per point ($n = 7$). The voltage dependence of the channel currents could be described by an exponential expression: $\langle I \rangle = \langle I_O \rangle \cdot \exp[(V/V') - 1]$, with a characteristic voltage $V' = 110$ mV and $\langle I_O \rangle = 50$ pA (O_1, $\Diamond$), 88 pA (O_2, $\triangle$), and 120 pA (O_3, $\bigcirc$). The single-channel conductances at 50 mV were 600 ± 30 pS (O_1), 935 ± 70 pS (O_2), and $1{,}250 \pm 130$ pS (O_3). Smaller current states (below 100 pS) were observed with a lower frequency of openings ($\blacklozenge$, $N \leq 50$).
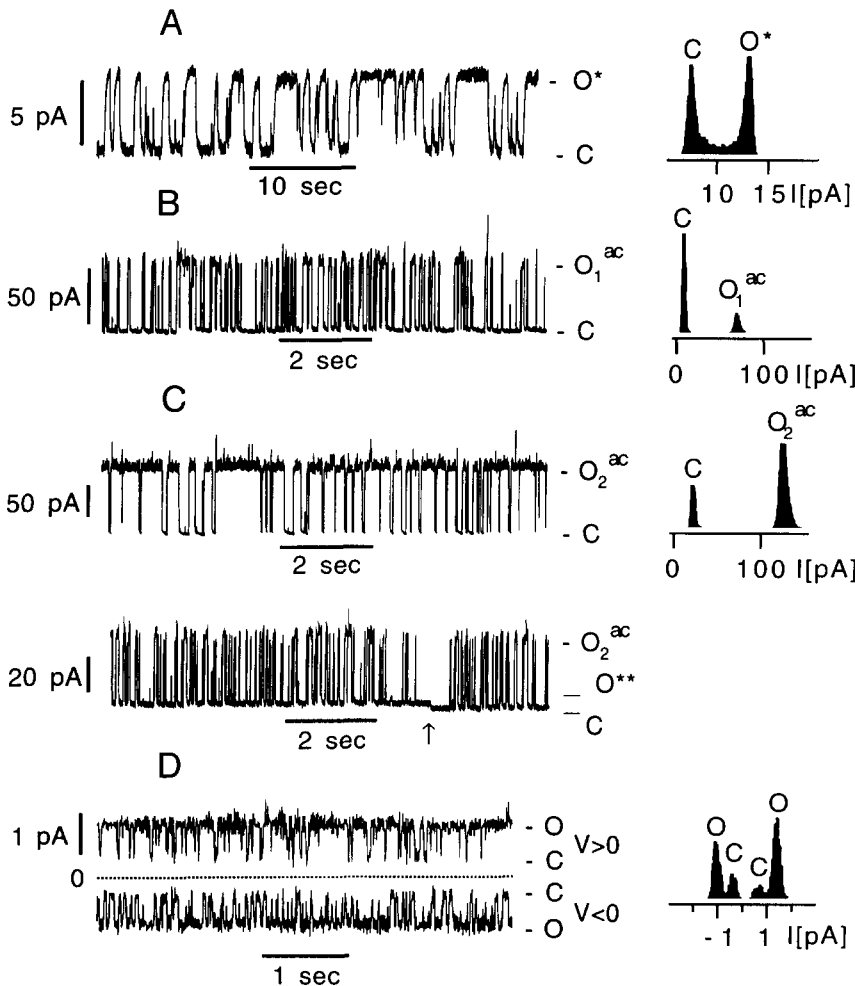
Fig. 9. Single-channel activity of acetylated melittin-TASP. The traces A, B, and C are typical sections from current recordings on small patch membranes (as described in Fig. 7), showing channel state O* (45 pS) 25 min after membrane formation (**A**) and O_1^{ac} (620 pS) and O_2^{ac} (1,000 pS) after ≥ 1 h (**B,C**) and the respective current histograms. The applied voltages were 125 mV in A, 100 mV in B and the upper trace of C, and 50 mV in the lower trace C (note the voltage dependence of the open times in the 2 traces of C). The arrow in the lower trace C indicates closing of the infrequent channel O** (100 pS). Trace **D** shows sections of the 7-pS channel, measured in large Montal–Mueller bilayers of DOPE:DOPC (4:1) with protein added only to 1 side of the membrane at almost 10 times lower concentration. The channel activates with both polarities (± 100 mV).

Fig. 10. Current–voltage characteristics of single-channel states formed by acetylated melittin-TASP on patch membranes of DOPE:DOPC (4:1) in 1 M NaCl, 10 mM Tris-HCl, pH 7.4. Channel currents were symmetrical with respect to voltage polarity. Open markers denote the maxima of multigaussian fits to current histograms of trace sections containing $N \geq 500$ events ($n = 3$). Full markers indicate single-channel currents from segments containing fewer events ($N \leq 50$). Dotted lines are exponential fits (cf. Fig. 8 caption) with a characteristic voltage $V' = 105$ mV and $\langle I_O \rangle = 41$ pA (O_1^{ac}, $\diamond$) and 58 pA (O_2^{ac}, $\triangle$). The single-channel conductances (at 100 mV) were 45 ± 5 pS (O^*, $\blacklozenge$), 100 ± 10 pS (O^{**}, $\blacktriangle$), 620 ± 40 pS (O_1^{ac}, $\diamond$), and $1,000 \pm 50$ pS (O_2^{ac}, $\triangle$). O^* occurred 15–30 min after membrane formation, the larger channels appeared simultaneously after ≥ 1 h. O^{**} appeared only in the presence of the large channels with openings in the second range. Open circles (O) indicate channels from trace segments with current amplitudes that do not fit the predominant states O_1^{ac} and O_2^{ac}.

ductances of $\langle O_1^{ac} \rangle = 620 \pm 40$ pS and $\langle O_2^{ac} \rangle = 1,000 \pm 50$ pS (Fig. 10). The conductances exhibited a similar voltage dependence to those of the unmodified protein with an *e*-fold increase of conductance every 105 ± 5 mV. Interestingly, within the established channel activity of O_1^{ac} and O_2^{ac}, a small, new state, O^{**}, similar to O^*, appeared occasionally (Fig. 9, arrow at lower trace C). It showed slow kinetics with τ_{open} and τ_{closed} in the second range and a channel conductance of $\langle O^{**} \rangle = 100 \pm 10$ pS, slightly larger than that of O^*. Generally, the channel states of the acetylated analogue were better defined compared to those of the unmodified melittin-TASP, as inferred from narrower Gaussian distributions in the channel current histograms, i.e., a decreased current noise of the open channel states. In addition, the channels could be reproducibly observed up to 9 h after membrane formation, which indicates the absence of membrane-damaging effects.

The gating kinetics of O_1^{ac} and O_2^{ac} were clearly regulated by voltage as demonstrated in Figure 9C, in the upper (50 mV) and in the lower (100 mV) trace. The mean open times increased with increasing voltages, whereas the mean lifetime of the closed states remained more or less constant. The transitions of the small channels of acetylated melittin-TASP, O^* (Fig. 9A), had longer lifetimes of around 0.5 s, as estimated from 2 experiments ($N \geq 50$). A critical voltage seems to be necessary for channel

activation, as is already evident from the macroscopic I-V curves (Fig. 6). Generally, the voltage dependencies of the channel conductances and the kinetics seemed to be more pronounced for the larger conductance states.

If the channels consist of aggregates of TASP molecules, channel activity should strongly depend on the protein concentration (Equation 5). In bilayers comprising less protein molecules, the number of channels formed by TASP aggregates should be diminished relative to the number of channels formed by TASP monomers. Indeed, the formation of bilayers from lipid solutions containing less protein (L:P > 1,000) drastically reduced the probability of observing a reasonable number of single channels within the given membrane area. Under these conditions, the use of small tip glass pipettes is unsuitable. Instead, larger membranes allow the use of less protein (larger L:P ratios) for the detection of single-channel events in a reasonable period of time and number of experiments. Therefore, single-channel activity was also measured on planar bilayers with larger membrane areas (diameter = 100 μm) under otherwise identical experimental conditions. Unfortunately, the current resolution is reduced. Acetylated melittin-TASP was chosen because, due to its reduced number of positive electrical charges, it might show a tendency to form the better defined and smaller channels.

Very small and ohmic single-channel current states with a conductance of 7 ± 1 pS were observed after the membrane formation (Fig. 9D). Although the protein was incorporated only from 1 side of the bilayer, the channel activity was established symmetrically at positive and negative voltages. Mean times of the open and closed states were in the 10-ms range.

The cyclized and the truncated (melittin$_{6-26}$)-TASP

Cyclized melittin-TASP. Here the potential structural flexibility of the template was reduced by cyclization in order to investigate whether this conformational restriction might create some new properties of channel behavior of melittin-TASP. However, the channel conductances and the opening/closing kinetics were in a similar range to those of the noncyclic TASP, except that there was a higher tendency to stabilize the smaller channel states as revealed by the state probabilities of the current histograms (see also Dhanapal et al., 1993).

Melittin$_{6-26}$-TASP. This truncated melittin-TASP was synthesized in order to test whether the first 5 amino acid residues of the N-terminal segments of the melittin chains play a significant role in the channel formation of the TASP. Compared to melittin-TASP, no significant changes of the single-channel properties of this TASP form have been observed.

Native melittin

For comparison, the channel activity of natural, monomeric melittin was measured under the same experimental conditions as used for TASP melittins on patch pipettes. Additional data of the channel characteristics of melittin in pure DOPC are taken from the literature (Pawlak, 1991; Pawlak et al., 1991). The membrane activity of melittin as revealed by electrical measurements can be characterized by 3 typical effects, shown in Figure 11. At low peptide concentrations, small and defined single channels could be observed (Fig. 11A). The channel conductance was 18 ± 3 pS and ohmic. Mean times for the open and closed states were in the second range, considerably longer than for the TASP molecules. Upon increasing the peptide concentration

Table 3. *Mean times of the open (τ_{open}) and closed states (τ_{close}) of different sized single-channel states of melittin-TASP (including the acetylated analogue) in small patch tip membranes*[a]

Melittin-TASP

Channel O_1 (600 pS)			Channel O_3 (1,250 pS)		
Voltage (mV)	τ_{close} (ms)	τ_{open} (ms)	Voltage (mV)	τ_{close} (ms)	τ_{open} (ms)
50	14 ± 5	12 ± 5	30	23 ± 5	23 ± 5
80	16 ± 5	7 ± 5	50	22 ± 5	40 ± 5
120	7 ± 5	140 ± 40	70	18 ± 5	56 ± 10

Acetylated melittin-TASP

Channel O_1^{ac} (620 pS)			Channel O_2^{ac} (1,000 pS)		
Voltage (mV)	τ_{close} (ms)	τ_{open} (ms)	Voltage (mV)	τ_{close} (ms)	τ_{open} (ms)
70	200 ± 50	8 ± 5	50	50 ± 20	12 ± 5
100	100 ± 20	31 ± 5	70	35 ± 20	35 ± 10
120	80 ± 20	44 ± 10	90	40 ± 20	80 ± 20
			100	40 ± 20	230 ± 50

Melittin

An "intermediate" channel[b]

Voltage (mV)	τ_{open} (ms)	τ_{close} (ms)
50	62 ± 10	102 ± 15
60	78 ± 10	93 ± 15
70	164 ± 15	105 ± 25
80	217 ± 60	99 ± 15
90	278 ± 60	97 ± 15

[a] In small patch tip membranes of DOPE:DOPC (4:1) bathed in 1 M NaCl, 10 mM Tris-HCl, pH 7.4. Data were obtained from current segments containing single transitions ($N \geq 200$-1,000, $n = 7$). Data for natural melittin are included.

[b] τ_{open} and τ_{close} correspond to melittin channels of an intermediate conductance of 110 pS (in 1.8 M NaCl, BLMs of DOPC) that were stationary over long time periods ($N > 250$, $n = 2$). The values are taken from Pawlak (1991).

and/or applied voltage, channel activity rose dramatically. Channels of larger conductances (175–300 pS) with a large variability in amplitudes appeared (Fig. 11B). They are still defined as sharp transitions, but fluctuate much faster, in the range of 50 ms. In addition, a continuously variable and apparently voltage-independent membrane conductance was superimposed on the discrete channel activity (Fig. 11B). This feature may reflect the membrane-damaging effects of melittin, which increased the probability of membrane rupture at high peptide concentrations and voltage. Another typical feature is shown in Figure 11C: apparently stationary single-channel traces were interrupted by burstlike, largely fluctuating sections, sometimes reaching conductances of 1–2 nS. The opening/closing kinetics of a distinct channel of intermediate conductance (60 pS at 1 M NaCl) were observed over long periods of time. Under these conditions, a voltage dependence of the gating kinetics could be observed that stabilizes the open state of the channel. Thus, τ_{open}

increased upon increasing the applied voltages and τ_{closed} remained constant (Table 3; Pawlak, 1991).

Dye release experiments

Melittin-TASP and native melittin were compared by measuring their overall efficiency for dye release from lipid vesicles. Figure 12 shows the characteristic curves normalized to the signal of 100% release after addition of detergent. The kinetics of dye release induced by melittin-TASP were similar to those induced by natural melittin, but comparable signal intensities had already been reached at protein concentrations about 20 times lower than for natural melittin. The final methanol content (maximum 1%) had no influence on the dye release.

Discussion

Structural measurements

The CD measurements show conclusively that the structural properties of the melittin-TASP in solvents as well as in lipid bilayers differ to some extent from those of natural melittin. Firstly, in aqueous solution, even at low peptide concentration, low ionic strength, and neutral pH, melittin-TASP exhibits a relatively high helix content, although under comparable conditions natural melittin remains in a random coil state (Talbot et al., 1979). The melittin-TASP shows a strong tendency to form large aggregates in an aqueous environment. Clearly, the template induces the peptide blocks to fold into helices, which will necessarily be amphipathic because they are long enough to be located at least partly on the hydrophobic segment of amino acids 1–20. In aqueous solution, the amphipathic helices of natural melittin assemble as tetramers shielding the hydrophobic areas by intermolecular contacts and yielding an overall hydrophilic surface of the peptide aggregate (Terwilliger & Eisenberg, 1982). In this respect, the tetramerization of natural melittin resembles the folding process of globular proteins (Goto & Hagihara, 1992; Hagihara et al., 1992). However, in melittin-TASP, the conformational constraints of the template prevent the individual helix blocks from arranging like the free, tetrameric melittin, i.e., as 2 pairs of antiparallel oriented dimers (see Terwilliger & Eisenberg, 1982). Consequently, nonshielded hydrophobic areas of the peptide blocks, comprising helical or nonhelical structures, can interact with equivalent partners of neighboring TASP molecules to form inter-TASP aggregates. In contrast, melittin-TASP remains molecularly dissolved in methanol with an increased helix content. The average secondary structure of nearly 60% α-helix content of melittin-TASP is identical in methanol and in lipid bilayers. Natural melittin exhibits 90% α-helical structure in methanol (Bazzo et al., 1988) and around 75% α-helix in the lipid membrane (Vogel, 1987). The quite notable difference in the helix content between melittin-TASP and free melittin in lipid bilayers corresponds to an average structural difference of about 5 amino acids per individual melittin chain (see Table 1). In the case of melittin$_{6-26}$-TASP, the CD data indicate about 11 amino acids per truncated melittin chain in a helical conformation. Even if we take into account the uncertainty of such an absolute structural interpretation of the CD data, the average helix content of this time and ensemble averaged protein structure seems to be too low to be
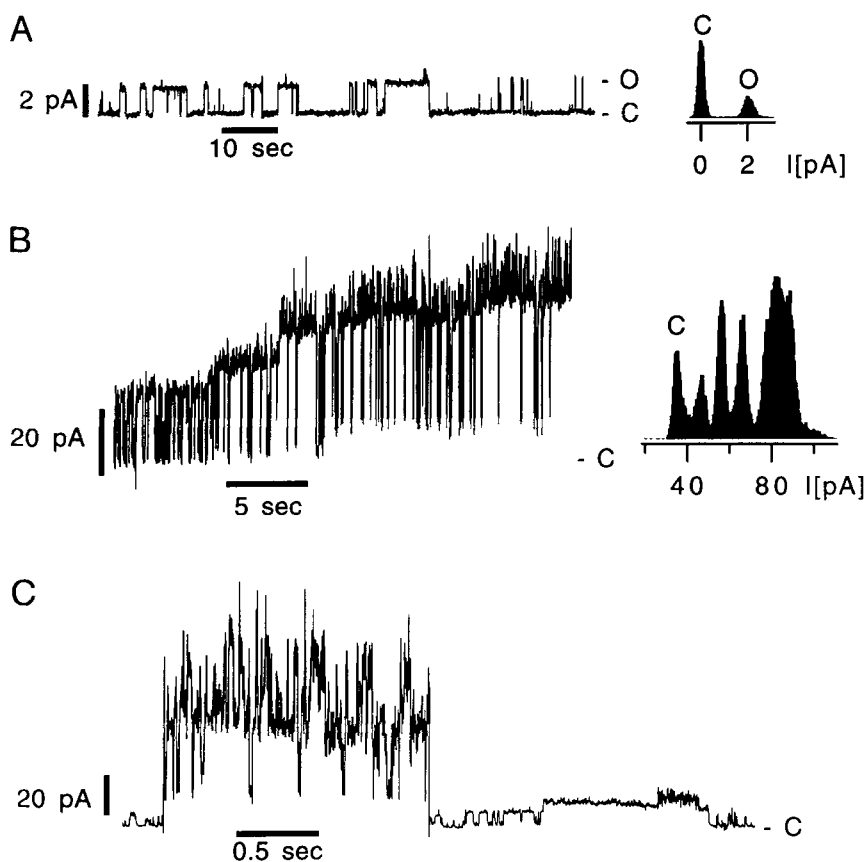
Fig. 11. Single-channel activity of natural melittin measured on patch bilayers (DOPE: DOPC [4:1] in 1 M NaCl, 10 mM Tris-HCl, pH 7.4). Melittin (in water) was added to the lipid monolayers before membrane formation (L:P $\geq$ 200 might be a [theoretical] upper limit of all peptide molecules captured in the lipid monolayers). The 3 traces show schematically the typical characteristics of melittin's channel activity (from $n = 5$) under these conditions: (A) formation of small, defined single channels of 15 pS conductance (recorded at 150 mV); (B) channels of larger conductances (175–300 pS) and large variability of amplitudes at constant voltage (120 mV), superimposed on a continuously varying current contribution; (C) (at 150 mV) discrete channel formation (about 50 pS) mixed with sections of a burstlike character, revealing ill-defined and quickly fluctuating conductances (here 300–600 pS).
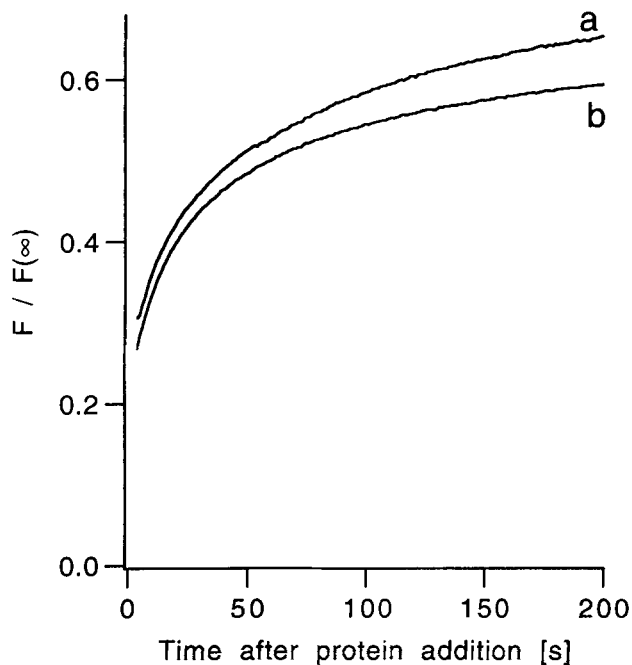

Fig. 12. 6-CF release from dye-loaded POPC vesicles with mean diameter 500 Å, induced by (a) 290 nM melittin and (b) 15 nM melittin-TASP. Experimental conditions were: lipid concentration = 80 μM, aqueous buffer = 100 mM NaCl, 10 mM Tris-HCl, pH 7.4.

arranged as uniformly membrane-spanning α-helices. Nevertheless, the truncated TASP forms ion channels.

The fluorescence spectra also indicate differences between the structures of melittin-TASP and natural melittin. Only a slight difference of the emission spectrum of the tryptophan was observed in the case of the TASP compound under the different solvent and membrane conditions ($\Delta\lambda_{max} \simeq 6$ nm), in contrast to natural melittin, where a large shift of the tryptophan emission wavelength ($\Delta\lambda_{max} = 17$–19 nm) occurs when transferring the peptide from an aqueous solution to a lipid-bound state (Dufourcq & Faucon, 1977; Vogel, 1981). This indicates that the tryptophan is probing a different environment in melittin-TASP than in natural melittin.

The affinity of melittin-TASP for lipid bilayers is high and orders of magnitude larger than for the natural peptide. This is indicative of the increased hydrophobic nature of the protein. However, due to the molecule's higher hydrophobicity, determination of the lipid partitioning is largely dependent on the experimental system. Adding melittin-TASP into an aqueous solution of lipid vesicles (as is done for the well water-soluble, natural peptide) apparently reduces the spontaneous membrane association. This effect might be due to protein aggregation in aqueous solution and to membrane-inactive protein aggregates. On the other hand, the strong affinity of the TASPs for lipid bilayers, when reconstituted from a lipid environment, is limited by repulsive protein–protein interactions at the membrane interface due to the large number of positive charges exposed

α-helical peptide bonds

unstructured peptide bonds

template
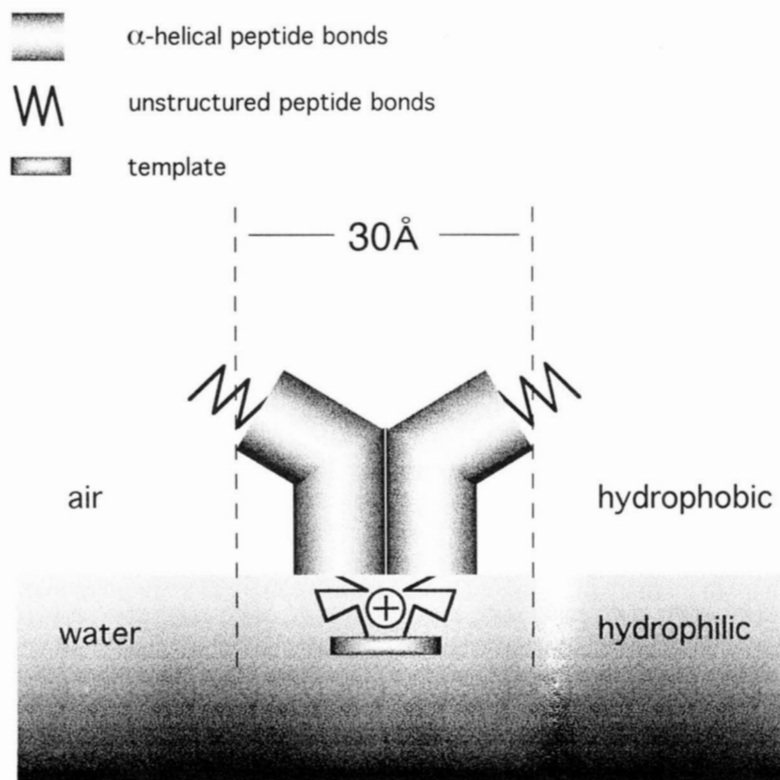
Fig. 13. Schematic side view of a melittin-TASP molecule in a self-assembled protein monolayer on an air-water interface. An area of 620 ± 60 Å^2 was measured after establishment of a bilayer-monolayer equivalent surface pressure of 32 mN/m, suggesting that all 4 peptide chains are preferentially oriented perpendicular to the interface. Assuming that 13 peptide bonds per melittin block form an α-helical structure (according to the CD measurements) comprising the hydrophobic residues 6–20 with a kink of an angle of 120° around the position of residue 12 (according to the crystal structure of Terwilliger & Eisenberg [1982]) and a helix diameter of 10 Å, an area of 30×20 Å$^2 = 600$ Å^2 was estimated per molecule. This value fits well with the observed area. The hydrophilic template and the strongly charged C-terminal segments of the melittin blocks (indicated by �) are assumed to extend into the water subphase.

to the aqueous solution. From the Gouy–Chapman approach, the effective charge of the melittin-TASP was derived as $z_{eff}^{mel\text{-}TASP} = 5.2$. This number is, firstly, much less than the expected formal protein charge, as already demonstrated for the natural melittin ($z_{eff}^{mel} = 1.9$), and, secondly, less than 4 times the effective charge of 1 melittin chain ($4 \times z_{eff}^{mel} = 7.6$). This is in line with a predicted reduction of the physical valency, z, of larger proteins, where the finite size of the molecule and the discreteness of the protein charge were explicitly considered (Stankowski, 1991). In this extended treatment, the "effective" reduction of z was theoretically shown to be more prominent with increasing protein size and increasing physical valency z of the molecule. Here, this trend is confirmed experimentally for melittin-TASP.

A central question regarding the functioning of melittin-TASP as a channel is whether the individual TASP molecules fold as helix bundles or as flat structures with the helices extending away from the template. In this context, the Langmuir experiments reveal some important aspects. Melittin-TASPs have a pronounced affinity for the air–water interface, which resembles a water–membrane interface. They can pack densely as a monolayer of high and stable surface pressure on the water surface, i.e., without loss of protein molecules into the aqueous subphase. This finding is quite remarkable and demonstrates for the first time that particular proteins comprise self-organizing properties. This has previously only been observed for lipid or lipidlike compounds (Roberts, 1990). The area of 620 Å^2 per TASP molecule at the bilayer–monolayer equivalent surface pressure, and the nearly identical area of 590 Å^2 of the truncated melittin$_{6-26}$-TASP, fit well with a conformation in which 4 kinked peptide helices of 10-Å diameter align perpendicularly

to the air–water interface (see Fig. 13 for a model). For a parallel alignment of the peptide segments on the water surface, one would expect a considerably larger area difference between the 2 differently sized molecules. The stable monolayer behavior might be due to the strong amphipathic nature of the protein in 2 respects: firstly, within the plane of the interface, it segregates hydrophobic and hydrophilic surfaces of neighboring peptide chains along the α-helical axes, and secondly, perpendicular to the interface, it segregates the strongly charged C-terminal peptide ends linked to the template and the more hydrophobic segments of amino acids 1–20. Additional infrared spectra of TASP monolayers, transferred to germanium substrates, revealed the amide I and II vibrational bands at wave numbers typical for an α-helical conformation (unpubl. results).

Functional measurements

The electrical measurements demonstrate the capability of melittin-TASP to function as defined ion channels in lipid bilayers. However, the channel activity was differently established depending on the reconstitution protocol. According to the macroscopic measurements, the channels are predominantly formed by either individual or by aggregated structures. Single-channel measurements of the various TASPs did not reveal one distinct channel state, but several differently sized channels with conductances of up to 1 nS. In the case of acetylated melittin-TASP at suitably low protein concentrations, channels with conductances as low as 7 pS have been observed, which, however, change to higher conductance levels slowly with time. It is reasonable to assume that the lowest conductance channels were formed by individual TASP molecules. Conductances of this

range have also been observed with other TASP molecules comprising authentic sequences of large, natural ion channel proteins (Montal et al., 1990; Grove et al., 1991). The change from channels of low conductance into channels of larger conductances is slow enough to be experimentally observed in the case of acetylated melittin-TASP. It may be interpreted as the intermolecular aggregation of single TASP molecules into larger structures within the lipid bilayer. Larger channel currents might be induced either by structures where parts of several TASPs contribute to a large channel or by the cooperative opening of several small channels within a cluster of TASP molecules. Such a cooperative process has been proposed for the channel openings of the bacterial outer membrane porins (Dargent et al., 1986) and also for the differently sized conductance levels of alamethicin pores (Bezrukov & Vodyanoy, 1993).

Once the large channels had been established, the initial, small channels disappeared completely and a new, but still small channel appeared occasionally (see O* [45 pS] and O** [100 pS] in Fig. 9C). These small states may be recognized as channels of the same origin but revealing different characteristics.

Native melittin forms defined ion channels in the conductance range of 18–300 pS and, in addition, less defined states of up to 1–2 nS. They all show a considerably larger variability in amplitude than the TASP channels. The observed conductances are in line with results of melittin in different bilayer systems (Tosteson & Tosteson, 1981; Hanke et al., 1983; Tosteson et al., 1985a) and of other small pore-forming peptides like the more hydrophobic, uncharged peptides of the alamethicin type (Gordon & Haydon, 1972; Menestrina et al., 1986; Vogel et al., 1993) and the charged peptides related to melittin, like mastoparans (Mellor & Sansom, 1990), δ-toxin (Mellor et al., 1988), and magainins (Duclohier et al., 1989). In addition to distinct channel formation, a voltage-independent conductance is superimposed, which clearly damages the membrane. This activity may be caused by molecules being associated with the membrane surface and not involved in channel formation. The attachment of 4 melittin chains to a template constrains the TASP channels to a few defined states, in contrast to the complexity of free melittin channels, which form multiple oligomeric states rather than a unique channel structure. A considerable contribution to the complexity of channel activity of the free peptide might result from the formation of channel aggregates where the individual monomers involved may be oriented parallel or antiparallel along the bilayer normal (Boheim et al., 1983; Furois-Corbin & Pullman, 1986; Guy & Ragunathan, 1988).

Template-assembled melittin can reproduce some typical features of the natural peptide, despite a reduced variability of channel states. Such features are formation of single channels in a similar range of conductances and a comparable voltage dependence of the macroscopic membrane conductance as expressed in terms of a gating charge number of around 1.3. The concentration dependence of channel formation of $m = 4$ for melittin decreased under certain conditions to $m = 1$ for melittin-TASP, consistent with the idea that the membrane conductance of melittin is induced by predominantly tetrameric channel structures. In addition, the propensity for aggregation seems to be characteristic of all melittin-TASPs tested. In all cases investigated, the distribution of conductance levels and the gating kinetics were more or less conserved, independently of whether the molecule was cyclized at the template, N-terminally truncated, or made even more hydrophobic by acetylation. In contrast, large changes of the channel properties were observed upon acetylation of the natural peptide (Stankowski et al., 1991): greatly prolonged lifetimes of the open channel states and an increase of the mean aggregation number from $m = 4$ to $m = 8$. These results demonstrate that the template stabilizes particular conformations of the TASP. Whether these are 4-helix bundle structures cannot yet be decided.

Both for melittin and for melittin-TASP, the open states of the channels are stabilized with respect to the closed states upon increasing voltages (see especially trace C of Fig. 9). Sensing of the transmembrane electric field by the pore in the open state may also be inferred from the fact that the single-channel conductances revealed a small, but perceptible voltage dependence (Fig. 10). Such a behavior is contrary to measurements with more hydrophobic and uncharged peptides, alamethicin, and synthetically designed model peptides (Boheim, 1974; Lear et al., 1988; Åkerfeldt et al., 1993). In the latter examples, voltage-dependent channel activation apparently results from an exclusive increase of the frequency of opening, i.e., a decreasing lifetime of the closed state. The increase of the opening rate was explained by models that concentrate on voltage-induced changes of the peptide helix orientations within the membrane (see Sansom [1991] for a review). These differences may indicate different processes of voltage gating for the charged and for the uncharged, hydrophobic peptides.

For a structural interpretation of the voltage-gating process, the following findings are important: (1) the rather low voltage dependence of the conductance of the TASP implies that only about a quarter of a gating charge per melittin chain is moved across the full bilayer thickness, (2) the open state of the channel is stabilized with increasing voltage, and (3) the channels can be activated symmetrically upon application of positive and negative voltages when the protein is added only to 1 side of the membrane. This means that all 4 C-terminal ends of the melittin blocks may be exposed on 1 side of the bilayer. These observations imply that the process of voltage gating is not the reorientation of peptide helices across the lipid bilayer resulting from the action of the electric field on the helix dipole moments. The monolayer experiments also indicate that the melittin helices may be oriented perpendicular to the air–water interface. Voltage activation of the channels may then be performed by voltage-induced, intramolecular structural transitions of a membrane-embedded, "pre-pore" conformation of melittin-TASP, as already proposed for the channel formation of natural melittin (Pawlak et al., 1991). In this model, the gating process would resemble the voltage activation of large, membrane-anchored channel proteins. Template association of the peptides may therefore be regarded as catalyzing the "pre-pore" state and may drastically increase the number of membrane-associated molecules directly involved in channel formation. The reduced spontaneous, and therefore voltage-independent, contributions to the membrane conductance may be a good indication of a strongly diminished pool of surface-associated molecules that do not penetrate the bilayer membrane (I-V curves of Fig. 6; Figs. 7, 9, 11).

Because of its surface activity and channel-forming properties, melittin is a strong hemolytic and antibiotic peptide (DeGrado et al., 1982; Tosteson et al., 1985b; Wade et al., 1990, 1992). Functional assays that directly compare melittin and melittin-TASP under the same experimental conditions reveal the influence of the template on the overall toxicity of the polypeptides. Compared to the free peptide, melittin-TASP is around 100

times more active with respect to channel formation and about 20 times more efficient in releasing dye molecules from lipid vesicles. The clear distinction between these 2 numbers indicates that the lytic properties are not exclusively related to channel formation but may also include surface-active effects. Accordingly, the effects that damage the integrity of the bilayer membrane are less pronounced for the TASP molecules than for the natural peptide.

Conclusion

The TASP approach is a versatile tool for constructing new synthetic polypeptides with specific properties. We have demonstrated that melittin-TASP can adopt preferential helical conformations in water, organic solvent, and lipid bilayer environments. The proteins show a large tendency to self-aggregate with increasing protein concentration both in water and in lipid membranes. When reconstituted in planar bilayer membranes (at low concentrations), single melittin-TASP molecules, with unidirectionally oriented peptide chains, reveal ion channel activity with certain characteristics comparable to the native peptide (channel conductance, voltage activation, voltage dependence, and gating kinetics). However, the results presented also indicate an important difference between free melittin and melittin-TASP; the attachment of 4 melittin chains to a template considerably reduces the complexity of the channel properties of free melittin to only a few defined channel states. The channel activity of the TASP was about 100 times more pronounced. Generally, the TASP approach may be a convenient tool to amplify structural and functional features of polypeptides known from their free monomeric states. It might be useful for the design of new, more powerful and specific antibiotics or the design of channel toxins with linked, specific recognition sites that may allow the regulation of the channel function by external triggers. The ability to form stable monolayers of melittin-TASP at air–water interfaces opens up the possibility of studying the self-assembly of pure protein layers at interfaces as well as a structural and functional investigation of the protein embedded in supported mono- or multilayers of lipid.

Materials and methods

Chemicals

DOPC, DOPE, and POPC were purchased from Avanti Polar Lipids (Birmingham, Alabama). All salts were from Fluka (Switzerland) and of grade MicroSelect. Methanol, ethanol, isopropanol, chloroform, hexane, decane, and hexadecane (all of UV-spectroscopy quality) were obtained from Merck (Germany). 6-CF was purchased from Molecular Probes (Eugene, Oregon) and used without further purification. For the synthesis, all the amino acids Boc-Lys-(Fmoc), Boc-Ala-OH, Boc-Cys-(Mob), Fmoc-Gly-OH, Fmoc-Ala-OH, Fmoc-Val-OH, Fmoc-Pro-OH, Fmoc-Ile-OH, Fmoc-Leu-OH, Fmoc-Gln-(Trt)-OH, Fmoc-Lys-(Boc)-OH, Fmoc-Arg-(Mtr)-OH, Fmoc-Trp-OH, Fmoc-Thr-OH, Fmoc-Ser-OH, the dipeptide Boc-Pro-Gly-OH, and the coupling reagents BOP, PyBOP, and the MBHA resin were from Bachem or Novabiochem (Switzerland), and the dansyl chloride, DMF, DCM, TFA, DIC, and HOBt from Fluka (Switzerland). Natural melittin was purchased from Mack (Germany) and purified as described by Vogel (1987).

Synthesis and purification of melittin-TASP

The melittin-TASP molecules were assembled using a combination of Boc and Fmoc strategies on a *p*-MBHA resin (Mutter et al., 1992; Tuchscherer et al., 1992). A high accessibility/low loading of the resin (0.3 mmol/g) was used in order to maximize coupling efficiencies in the assembly of the helices. The synthesis of the template molecule was performed manually, using Nα-Boc-protected amino acids, with Mob for Cys and Fmoc for Lys side-chain protection. Boc-Pro-Gly-OH was introduced as a dipeptide using BOP reagent. All the other couplings were performed in a 2 M solution with 3 equivalents of DIC/HOBt or BOP/HOBt in the presence of DIPEA. The N-terminus of the template was acetylated using acetic anhydride and pyridine.

For the construction of the melittin helices, Nϵ-Fmoc groups were removed by treatment with 50% piperidine in DCM. The number of moles of resulting free N-termini was then calculated by spectrophotometric determination of the liberated dibenzofulvene. Side chains of trifunctional amino acids were protected as follows: Gln (Trt), Arg (Mtr), Lys (Boc), Ser (tBu), and Thr (tBu). The parallel assembly of the peptide blocks was carried out semiautomatically and was followed by the quantitative ninhydrin test. Repetitive coupling was carried out to ensure the high coupling yields for each step and, in the case of incomplete coupling reactions, acetylation was subsequently performed.

The TASP molecules were cleaved from the resin by treatment with TFMSA/TFA/DMS/EDT/H$_2$O (Dhanapal et al., 1993) and then subjected to multiple purification steps by RP-HPLC on C4 (Vydac, California) and C2 (Macherey-Nagel, Germany) columns. This method allowed the isolation of milligram quantities of purified TASP molecules but in low yields (2–5%). Acetylated melittin-TASP was obtained by the reaction of purified linear melittin-TASP (4 mg), dissolved in 500 μL of distilled DMF, 250 μL pyridine, and 250 μL of acetic anhydride for 24 h at room temperature. The homogeneity of the protein after purification was confirmed by RP-HPLC. Amino acid analysis revealed the expected composition. Laser desorption ionization mass spectrum analysis (Fig. 14) confirmed the expected molecular weight (MW = 12,374). Melittin-TASP was cyclized according to a method described by Tuchscherer et al. (1992) and purified by preparative RP-HPLC. Representative chromatograms are published elsewhere (Dhanapal et al., 1993).

The concentration of melittin-TASP in solution was determined by UV spectroscopy using 4 times the absorption coefficient of tryptophan at 280 nm, $\epsilon = 4 \times 5{,}570$ M^{-1} cm^{-1} = 22,280 M^{-1} cm^{-1} (Wetlaufer, 1962) and by amino acid analysis (Chang & Knecht, 1986). The protein solutions for the experiments were routinely prepared from stock solutions of ~0.5 mg/mL melittin-TASP in methanol. The protein solutions were diluted by adding small aliquots of the stock solution (while stirring) into the selected solvent. The final methanol concentration never exceeded 3%.

CD and fluorescence measurements

CD measurements were performed in quartz cuvettes on an AVIV 62 DS spectropolarimeter (Aviv, Lakewood, New Jersey), calibrated with *d*(+)-10-camphorsulfonic acid. The optical path-lengths of the cuvettes were 1 mm or 10 mm, as indicated in the figures. For each wavelength scan (data were sampled 3 s for every nm), the absorption of the sample was simultaneously
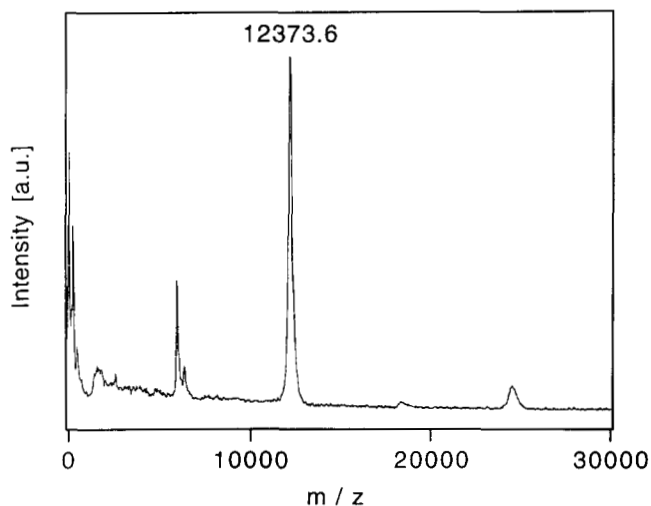
Fig. 14. Laser desorption ionization mass spectrum of melittin-TASP after final, extensive purification with RP-HPLC, using sinapinic acid as a matrix. The mass spectrum confirmed the expected molecular weight (MW = 12,374). Measurements were performed as described by Dörner et al. (1992).

recorded as a control for scattered light. The sample cuvettes were continuously stirred during the measurements. [θ] represents the mean ellipticity per residue in deg cm^2 dmol^{-1}. For each reported CD spectrum, at least 3 separate scans were taken, averaged, and corrected for the baseline and the baseline drift at 260 nm. The actual concentrations of the sample solutions were determined by amino acid analysis. The percentage of α-helix was evaluated by fitting the particular experimental CD spectrum by a set of reference proteins as described elsewhere (Vogel, 1987). The values of the protein helix content, fitted to whole spectra, corresponded within ±2% to the values obtained when using only the measured [θ]$_{222}$ and $-30,000$ deg·cm^2· dmol^{-1} as a base for 100% α-helix per residue of the peptide blocks (Chen et al., 1974).

Fluorescence measurements were performed in 1-cm × 1-cm quartz cells using a Spex fluorimeter model 1681. The Trp fluorescence of the protein was excited at 280 nm (slit width 1 mm) and detected between 285 nm and 450 nm (slit width 5 mm). Spectra were baseline corrected using samples without TASP under otherwise identical experimental conditions. Aqueous solutions were buffered with 10 mM Tris-HCl, pH 7.4. The solutions had been carefully degassed. In all experiments, the temperature was maintained at 25 ± 0.2 °C.

Conductance measurements on planar lipid bilayers

Measurements of single-channel conductances with a high current resolution were performed on planar lipid bilayers on the tips of patch pipettes as described by Coronado and Latorre (1983). Borosilicate glass capillaries (inner/outer diameter = 0.8/1.5 mm, Science Products, Germany) were pulled using a 3-step heating protocol (see Hamill et al., 1981) on a Flaming/Brown micropipette puller, model P-87 (Sutter Co., USA) and used without further treatment. The patch pipettes had tip diameters of 1–2 μm, as estimated from the open tip resistances and from scanning electron microscopy pictures. The protein was recon-

stituted by adding small amounts of the protein stock solution in methanol to a 1-mg/mL DOPE:DOPC (4:1) solution in chloroform, reaching final lipid:protein ratios between 1,000 and 5,000. Bilayers were formed by apposition of lipid–protein monolayers that had been spread from the organic L:P solutions on the air–water interface of Teflon cups (surface area of 8 cm^2). The cups contained 5 mL of buffer. In most of the experiments, single-channel activity was established just a few minutes after the membrane formation, but only if the membrane had been initialized with a high voltage (150–250 mV). Seal resistances of the membranes were in the range of 2–20 GΩ.

Alternatively, bilayers of the same lipid composition were formed across a hole (diameter 100 μm) in a thin Teflon septum according to Montal and Mueller (1972). This method allows the formation of bilayers that contain protein only on 1 side. In addition, a lower protein:lipid ratio can be used for single-channel recording because of the larger membrane area (8 × 10^{-3} mm^2).

Macroscopic membrane conductance, induced by a statistically significant number of channels, was studied on decane-containing BLMs (Mueller et al., 1962) with large membrane areas (0.4 mm^2). The bilayers were formed from DOPC as described by Pawlak et al. (1991). The membranes separated 2 compartments (each of 10 mL of volume) in order to minimize protein adsorption to the walls. After protein addition, the compartments were well stirred for several minutes and membrane conductance was subsequently recorded upon application of voltage ramps (0 to ±200 mV, slope = 100 mV/min). The current–voltage curves became stationary after about 1 h.

Routinely, all experiments were performed at room temperature (22–25 °C) in 1 M NaCl, 10 mM Tris-HCl, pH 7.4, unless otherwise stated.

The electronic set-up has been described recently (Pawlak et al., 1994). The current signals were measured via a pair of Ag/AgCl electrodes, using the amplifiers RK-300 for patch clamp and BLM-120 for BLM measurements (both Biologic, France). The headstages contained 10^8 Ω and 10^{10} Ω feedback resistances. Voltage polarity corresponds to the side of the working electrode (inside the patch pipette), the reference electrode in the bath being grounded. For the BLM measurements, positive voltage corresponds to the side of protein addition (*cis*). The current signals were filtered with a 5-pole cut-off frequency of 1 kHz and recorded on a digital tape recorder. Segments of the current recordings were sampled at a rate of 0.5 ms per point to a computer hard disk. Single-channel conductances were derived from multigaussian fits to current histograms. Mean open and closed state times were evaluated from monoexponential fits to segments of single transitions (at least 200–1,000 events). N denotes the number of events per current trace segment and n the number of experiments. The indexation of the different channels by numbers was chosen with respect to similarities in channel conductances and gating kinetics.

Preparation of the lipid samples

SUV were prepared from POPC by sonication of 0.3-mL dispersions of 1 mg/mL lipid in aqueous buffer. Alternatively, small unilamellar vesicles were produced by adding small amounts of a concentrated stock solution in methanol of the desired lipid:protein ratio to the sample compartments in the experiments, similarly as described for pure lipids by Szoka and Papahadjopoulos (1980). For measurements at different pro-

tein:lipid ratios, the volume of methanol added was kept constant and did not exceed 1% of the sample volume. LUV of POPC were prepared by extruding a lipid dispersion of 5 mg/mL of POPC repeatedly through polycarbonate filters with pore sizes of either 500 Å or 1,000 Å (as indicated) until turbidity disappeared and remained constant as revealed by UV absorption spectra. For the dye release experiments (see below), the lipid dispersion was freeze-thawed 3 times before extrusion to achieve a good spatial distribution of the dye. Aqueous buffer was 10 mM Tris-HCl, pH 7.4, at room temperature (22-25 °C), if not otherwise stated.

Dye-release experiments

Dye-loaded unilamellar lipid vesicles with a mean diameter of 500 Å were prepared by extrusion in the presence of 6-CF dye at a self-quenching concentration: 10 mg/mL POPC, 50 mM 6-CF, 135 mM NaOH, 10 mM Tris-HCl, pH 7.4. Untrapped dye was removed by passing the vesicle solutions over PD-10 Sephadex G-25 columns (Pharmacia, Sweden) using 100 mM NaCl, 1 mM EDTA, 10 mM Tris-NaCl, pH 7.4, as eluent.

For the experiment, small amounts of freshly prepared, dye-loaded vesicle solution were added, with stirring, to 1.5 mL of aqueous melittin or melittin-TASP solutions, which were diluted from concentrated protein solutions in methanol (containing the same molar amounts of protein for the 2 cases). The time of addition is indicated by time 0. The release of dye molecules was followed spectroscopically by the increase of the 6-CF sample fluorescence (excitation at 495 nm, emission at 515 nm). The final signal, $F(\infty)$, corresponds to a 100% release determined after addition of a small amount of detergent (30 μL of a 10% Triton X-100 solution). The fluorescence curves were normalized to the values of $F(\infty)$ (for the method, see also Schwarz & Robert [1990]). Aqueous buffer was 100 mM NaCl, 1 mM EDTA, 10 mM Tris-HCl, pH 7.4, at room temperature (22-25 °C).

Acknowledgments

References

Akabas MH, Stauffer DA, Xu M. 1992. Acetylcholine receptor channel structure probed in cysteine-substitution mutants. *Science 258*:307-310.

Åkerfeldt KS, Kim RM, Camac D, Groves JT, Lear JD, DeGrado WF. 1992. Tetraphilin: A four-helix proton channel built on a tetraphenylporphyrin framework. *J Am Chem Soc 114*:9656-9657.

Åkerfeldt KS, Lear JD, Wasserman ZR, Chung LA, DeGrado WF. 1993. Synthetic peptides as models for ion channel peptides. *Acc Chem Res 26*:191-197.

Bazzo R, Tappin MJ, Pastore A, Harvey TS, Carver JA, Campell ID. 1988. The structure of melittin. A ^{1}H-NMR study in methanol. *Eur J Biochem 173*:139-146.

Beschiaschvili G, Baeuerle HD. 1991. Effective charge of melittin upon interaction with POPC vesicles. *Biochim Biophys Acta 1068*:195-200.

Beschiaschvili G, Seelig J. 1990. Melittin binding to mixed phosphatidylglycerol/phosphatidylcholine membranes. *Biochemistry 29*:52-58.

Bezrukov SM, Vodyanoy I. 1993. Probing alamethicin channels with water-soluble polymers. *Biophys J 64*:16-25.

Boheim G. 1974. Statistical analysis of alamethicin channels in black lipid membranes. *J Membr Biol 19*:277-303.

Boheim G, Hanke W, Jung G. 1983. Alamethicin pore formation: Voltage-dependent flip-flop of α-helix dipoles. *Biophys Struct Mech 9*:181-191.

Boheim G, Kolb A. 1978. Analysis of the multi-pore system of alamethicin in a lipid membrane: Voltage-jump current-relaxation experiments. *J Membr Biol 38*:99-150.

Chang J, Knecht R. 1986. Liquid chromatographic determination of amino acids after gas phase hydrolysis and derivatization with (dimethyl-amino)azobenzenesulfanylchloride. *Anal Chem 58*:2375-2379.

Changeux JP, Galzi JL, Devillers-Thiéry A, Bertrand D. 1992. The functional architecture of the acetylcholine nicotinic receptor explored by affinity labelling and site-directed mutagenesis. *Q Rev Biophys 25*:395-432.

Chen YH, Yang JT, Chau KH. 1974. Determination of the helix and β form of proteins in aqueous solution by circular dichroism. *Biochemistry 13*: 3350-3359.

Chung LA, Lear JD, DeGrado WF. 1992. Fluorescence studies of the secondary structure and orientation of a model ion channel peptide in phospholipid vesicles. *Biochemistry 31*:6608-6616.

Coronado R, Latorre R. 1983. Phospholipid bilayers made from monolayers on patch-clamp pipettes. *Biophys J 43*:231-236.

Cowan SW, Schirmer T, Rummel G, Steiert M, Ghosh R, Pauptit RA, Jansonius JN, Rosenbusch JP. 1992. Crystal structures explain functional properties of two *E. coli* porins. *Nature 358*:727-733.

Dargent B, Hofmann W, Pattus F, Rosenbusch JP. 1986. The selectivity filter of voltage-dependent channels formed by phosphoporin (PhoE proterin) from *E. coli*. *EMBO J 5*:773-778.

DeGrado WF, Musso GF, Lieber M, Kaiser ET, Kezdy FJ. 1982. Kinetics and mechanism of hemolysis induced by melittin and by a synthetic melittin analogue. *Biophys J 37*:329-338.

Dempsey CE. 1990. The actions of melittin. *Biochim Biophys Acta 1031*: 143-161.

Dhanapal B, Meseth U, Pawlak M, Tuchscherer G, Vogel H, Mutter M. 1993. Chemical synthesis and functional characterization of melittin-TASP molecules. In: Epton R, ed. *Innovations and perspectives of solid phase peptide synthesis: 3rd SPPS*. Oxford, UK: Oxford University Press.

Dörner B, Cari RI, Mutter M, Labhardt AM, Steiner V, Rink H. 1992. New roots to artificial proteins applying the TASP concept. In: *2nd International Conference of Innovations and Perspectives of Solid Phase Peptide Synthesis 1992*. Andover, UK: Intersept Ltd. pp 163-170.

Duclohier H, Molle G, Spach G. 1989. Antimicrobial peptide magainin 1 from *Xenopus* skin forms anion-permeable channel in planar lipid bilayers. *Biophys J 56*:1017-1021.

Dufourcq J, Faucon JF. 1977. Intrinsic fluorescence study of lipid-protein interactions in membrane models: Binding of melittin, an amphipathic peptide, to phospholipid vesicles. *Biochim Biophys Acta 467*:1-11.

Durell SR, Guy HR. 1992. Atomic scale structure and functional models of voltage-gated potassium channels. *Biophys J 62*:238-250.

Furois-Corbin S, Pullman A. 1986. Theoretical study of the packing of α-helices by energy minimization: Effect of the length of the helices on the packing energy and on the optimal configuration of a pair. *Chem Phys Lett 123*:305-310.

Gordon LGM, Haydon DA. 1972. The unit conductance channel of alamethicin. *Biochim Biophys Acta 255*:1014-1018.

Görne-Tschelnokow U, Strecker A, Kadik C, Naumann D, Hucho F. 1994. The transmembrane domains of the nicotinic acetylcholine receptor contain α-helical and β structures. *EMBO J 13*:338-341.

Goto Y, Hagihara Y. 1992. Mechanism of the conformational transition of melittin. *Biochemistry 31*:732-738.

Grove A, Mutter M, Rivier JE, Montal M. 1993a. Template assembled synthetic proteins designed to adopt a globular four-helix bundle conformation form ionic channels in lipid bilayers. *J Am Chem Soc 115*: 5919-5924.

Grove A, Tomich JM, Iwamoto T, Montal M. 1993b. Design of a functional calcium channel protein: Inferences about an ion channel-forming motif derived from the primary structure of voltage-gated calcium channels. *Protein Sci 2*:1918-1930.

Grove A, Tomich JM, Montal M. 1991. A blueprint for the pore-forming structure of voltage-gated calcium channels. *Proc Natl Acad Sci USA 88*:6418-6422.

Guy HR, Ragunathan G. 1988. Structural models for membrane insertion and channel formation by antiparallel alpha helical membrane peptides. In: Pullman A, Jortner J, Pullman B, eds. *Transport through membranes: Carriers, channels and pumps*. Dordrecht: Kluwer Academic Publishers. pp 369-379.

Hagihara Y, Kataoka M, Aimoto S, Goto Y. 1992. Charge repulsion in the conformational stability of melittin. *Biochemistry 31*:11908-11914.

Hamill OP, Marty A, Neher E, Sakmann B, Sigworth FJ. 1981. Improved

patch-clamp techniques for high-resolution current recording from cells and cell-free membrane patches. *Pflügers Arch 391*:85-100.

Hanke W, Methfessel C, Wilmsen HU, Katz E, Jung G, Boheim G. 1983. Melittin and a chemically modified trichotoxin form alamethicin-type multi-state pores. *Biochim Biophys Acta 727*:108-114.

Hiemenz PC. 1986. *Principles of colloid and surface chemistry*. New York: Marcel Dekker.

Hille B. 1992. *Ionic channels of excitable membranes*. Sunderland, Massachusetts: Sinauer Associates.

Imoto K, Busch C, Sakmann B, Mishina M, Konno T, Nakai J, Bujo H, Mori Y, Fukuda K, Numa S. 1988. Rings of negatively charged amino acids determine the acetylcholine receptor channel conductance. *Nature 335*: 645-648.

Inagaki F, Shimada I, Kawaguchi K, Hirano M, Terasawa I, Ikura T, Go N. 1989. Structure of melittin bound to perdeuterated dodecylphosphocholine micelles as studied by two-dimensional NMR and distance geometry calculation. *Biochemistry 28*:5985-5991.

Israelachvili S, Marcelja S, Horn RG. 1980. Physical principles of membrane organization. *Q Rev Biophys 13*:121-200.

Lang H, Duschl C, Vogel H. 1994. A new class of thiolipids for the attachment of lipid bilayers on gold surfaces. *Langmuir 10*:187-210.

Latorre R, Alvarez O. 1981. Voltage-dependent channels in planar lipid bilayer membranes. *Physiol Rev 61*:77-150.

Lear JD, Wasserman ZR, DeGrado WF. 1988. Synthetic amphiphilic peptide models form protein ion channels. *Science 240*:1177-1181.

Massey JB, Pownall HJ. 1986. Thermodynamics of apolipoprotein-phospholipid association. *Methods Enzymol 128*:403-413.

Mellor IR, Sansom MSP. 1990. Ion-channel properties of mastoparan, a 14-residue peptide from wasp venom, and of MP3 a 12-residue analogue. *Proc R Soc Lond B 239*:383-400.

Mellor IR, Thomas DH, Sansom MSP. 1988. Properties of ion channels formed by *Staphylococcus aureus* δ-toxin. *Biochim Biophys Acta 942*: 280-294.

Menestrina G, Voges KP, Jung G, Boheim G. 1986. Voltage-dependent channel formation by rods of helical polypeptides. *J Membr Biol 93*:111-132.

Meseth U, Pawlak M, Dhanapal B, Mutter M, Vogel H. 1993. Melittin-TASP: A structure-function approach for studying channel-forming proteins. *Medical microbiology and immunology (second international workshop on pore-forming toxins) 182*:205.

Miller C. 1993. Potassium selectivity in proteins: Oxygen cage or in the face? *Science 261*:1692-1693.

Montal M. 1990. Molecular anatomy and molecular design of channel proteins. *FASEB J 4*:2623-2635.

Montal M, Montal MS, Tomich JM. 1990. Synporins — Synthetic proteins that emulate the pore structure of biological ionic channels. *Proc Natl Acad Sci USA 87*:6929-6933.

Montal M, Mueller P. 1972. Formation of bimolecular membranes from lipid monolayers and a study of their electrical properties. *Proc Natl Acad Sci USA 69*:3561-3566.

Mueller P, Rudin DO, Ti Tien H, Wescott WC. 1962. Reconstitution of cell membrane structure *in vitro* and its transformation into an excitable system. *Nature 194*:979.

Mutter M, Tuchscherer GG, Miller C, Altmann KH, Carey RI, Wyss DF, Labhardt AM, Rivier JE. 1992. Template-assembled synthetic proteins with four-helix-bundle topology. Total chemical synthesis and conformational studies. *J Am Chem Soc 114*:1463-1470.

Mutter M, Vuilleumier S. 1989. A chemical approach to protein design: Template-assembled synthetic proteins (TASP). *Angew Chem Int Ed Engl 28*:535-554.

Numa S. 1989. A molecular view of neurotransmitter receptors and ionic channels. *Harvey Lect 83*:121-165.

Pawlak M. 1991. Melittininduzierte Porenbildung in planaren Lipidmembranen unter dem Einfluß elektrischer Spannungen [thesis]. Basel, Switzerland: Faculty of Sciences, University of Basel.

Pawlak M, Kuhn A, Vogel H. 1994. Pf3 coat protein forms voltage-gated ion channels in planar lipid bilayers. *Biochemistry 33*:283-290.

Pawlak M, Stankowski S, Schwarz G. 1991. Melittin induced voltage-dependent conductance in DOPC lipid bilayers. *Biochim Biophys Acta 1062*:94-102.

Peled H, Shai Y. 1993. Membrane insertion and self-assembly within phospholipid membranes of synthetic segments corresponding to the H-5 region of the shaker K$^+$ channel. *Biochemistry 32*:7879-7885.

Quay SC, Condie CC. 1983. Conformational studies of aqueous melittin: Thermodynamic parameters of the monomer-tetramer self-association reaction. *Biochemistry 22*:695-700.

Rapoport D, Shai Y. 1991. Interaction of fluorescently labeled pardaxin and its analogues with lipid bilayers. *J Biol Chem 266*:23769-23775.

Roberts G. 1990. *Langmuir-Blodgett films*. New York: Plenum Press.

Sansom MSP. 1991. The biophysics of peptide models of ion channels. *Prog Biophys Mol Biol 55*:139-235.

Schwarz G, Beschiaschvili G. 1988. Kinetics of melittin self-association in aqueous solution. *Biochemistry 27*:7826-7831.

Schwarz G, Beschiaschvili G. 1989. Thermodynamic and kinetic studies on the association of melittin with a phospholipid bilayer. *Biochim Biophys Acta 979*:82-90.

Schwarz G, Blochmann U. 1993. Association of the wasp venom peptide mastoparan with electrically neutral lipid vesicles. *FEBS Lett 318*:172-176.

Schwarz G, Robert CH. 1990. Pore formation kinetics in membranes, determined from the release of marker out of liposomes or cells. *Biophys J 58*:577-583.

Schwarz G, Stankowski S, Rizzo V. 1986. Thermodynamic analysis of incorporation and aggregation in a membrane: Application to the pore-forming peptide alamethicin. *Biochim Biophys Acta 861*:141-151.

Stankowski S. 1991. Surface charging by large multivalent molecules. Extending the standard Gouy-Chapman theory. *Biophys J 60*:341-351.

Stankowski S, Pawlak M, Kaisheva E, Robert CH, Schwarz G. 1991. A combined study of aggregation, membrane affinity and pore activity of natural and modified melittin. *Biochim Biophys Acta 1069*:77-86.

Szoka F, Papahadjopoulos D. 1980. Comparative properties and methods of preparation of lipid vesicles (liposomes). *Annu Rev Biophys Bioeng 9*:467-508.

Talbot JC, Dufourcq J, de Bony J, Faucon JF, Lussan C. 1979. Conformational change and self association of monomeric melittin. *FEBS Lett 102*: 191-193.

Tanford C. 1980. *The hydrophobic effect: Formation of micelles and biological membranes*. New York: Wiley.

Terwilliger TC, Eisenberg D. 1982. The structure of melittin: Interpretation of the structure. *J Biol Chem 257*:6016-6022.

Terwilliger TC, Weissman L, Eisenberg D. 1982. The structure of melittin in the form I crystals and its implication for melittin's lytic and surface activities. *Biophys J 37*:353-361.

Tosteson MT, Alvarez O, Tosteson DC. 1985a. Peptides as promoters of ion-permeable channels. *Regul Pept 8*(Suppl 4):39-45.

Tosteson MT, Holmes SJ, Razin M, Tosteson DC. 1985b. Melittin lysis of red cells. *J Membr Biol 87*:35-44.

Tosteson MT, Tosteson DC. 1981. Melittin forms channels in lipid bilayers. *Biophys J 36*:109-116.

Tuchscherer G, Servis C, Corradin G, Blum U, Rivier J, Mutter M. 1992. Total chemical synthesis, characterization, and immunological properties of an MHC class I model using the TASP concept for protein de novo design. *Protein Sci 1992*:1377-1386.

Unwin N. 1993a. Neurotransmitter action: Opening of ligand-gated ion channels. *Cell 72*(10):31-41.

Unwin N. 1993b. Nicotinic acetylcholine receptor at 9 Å resolution. *J Mol Biol 229*:1101-1124.

Vogel H. 1981. Incorporation of melittin into phosphatidylcholine bilayers. *FEBS Lett 134*:37-42.

Vogel H. 1987. Comparison of the conformation and orientation of alamethicin and melittin in lipid membranes. *Biochemistry 26*:4562-4572.

Vogel H, Jähnig F. 1986. The structure of melittin in membranes. *Biophys J 50*:573-582.

Vogel H, Nilsson L, Rigler R, Meder S, Boheim G, Beck W, Jung G. 1993. Structural fluctuations between two conformational states of a transmembrane helical peptide are related to its channel-forming properties in planar lipid membranes. *Eur J Biochem 212*:305-313.

Vogel H, Nilsson L, Rigler R, Voges KP, Jung G. 1988. Structural fluctuations of a helical polypeptide traversing a lipid bilayer. *Proc Natl Acad Sci USA 85*:5067-5071.

Wade D, Andreu D, Mitchell SA, Silveira AMV, Boman A, Boman HG, Merrifield RB. 1992. Antibacterial peptides designed as analogs or hybrids of cecrobins and melittin. *Int J Peptide Protein Res 40*:429-436.

Wade D, Boman A, Wåhlin B, Dain CM, Andreu D, Boman HG, Merrifield RB. 1990. All-D amino acid containing channel-forming antibiotic peptides. *Proc Natl Acad Sci USA 87*:4761-4765.

Weiss MS, Abele U, Weckesser J, Welte W, Schiltz E, Schulz GE. 1991. Molecular architecture and electrostatic properties of a bacterial porin. *Science 254*:1627-1630.

Wetlaufer DB. 1962. Ultraviolet spectra of proteins and amino acids. *Adv Protein Chem 17*:303-390.